Neuro-Oncology

XX(XX), 1–13, 2021 | doi:10.1093/neuonc/noaa297 | Advance Access date 23 December 2020

Identification of diverse tumor endothelial cell populations in malignant glioma

Jeff C. Carlson†, Manuel Cantu Gutierrez†, Brittney Lozzi, Emmet Huang-Hobbs, Williamson D. Turner, Burak Tepe, Yiqun Zhang, Alexander M. Herman, Ganesh Rao, Chad J. Creighton, Joshua D. Wythe†, and Benjamin Deneen†

Program in Developmental Biology, Baylor College of Medicine, Houston, Texas (J.C.C., M.C.-C., J.D.W., B.D.); Center for Cell and Gene Therapy, Baylor College of Medicine, Houston, Texas (J.C.C., B.L., E.H.-H., B.D.); Department of Molecular Physiology and Biophysics, Baylor College of Medicine, Houston, Texas (M.C.-C., W.D.T., A.M.H., J.D.W.); Cardiovascular Research Institute, Baylor College of Medicine, Houston, Texas (M.C.-C., W.D.T., A.M.H., J.D.W.); Dan L Duncan Cancer Center, Division of Biostatistics, Baylor College of Medicine, Houston, Texas (Y.Z., C.J.C.); The Integrative Molecular and Biomedical Sciences Graduate Program, Baylor College of Medicine, Houston, Texas (E.H.-H.); Graduate Program in Translational Biology and Molecular Medicine, Baylor College of Medicine, Houston, Texas (W.D.T., J.D.W.); Department of Molecular and Human Genetics, Baylor College of Medicine, Houston, Texas (B.T.); Department of Medicine, Baylor College of Medicine, Houston, Texas (C.J.C.); Department of Neurosurgery, Baylor College of Medicine, Houston, Texas (G.R., B.D.)

†These authors contributed equally to this work.

Corresponding Authors: Joshua D. Wythe, PhD, Cardiovascular Research Institute, One Baylor Plaza, Baylor College of Medicine, Houston, TX 77030, USA (wythe@bcm.edu); Benjamin Deneen, PhD, Center for Cell and Gene Therapy, One Baylor Plaza, Baylor College of Medicine, Houston, TX 77030, USA (deneen@bcm.edu).

Abstract

Background. Glioblastoma is the most common and aggressive type of primary brain tumor, as most patients succumb to the disease less than two years after diagnosis. Critically, studies demonstrate that glioma recruits surrounding blood vessels, while some work suggests that tumor stem cells themselves directly differentiate into endothelial cells, yet the molecular and cellular dynamics of the endothelium in glioma are poorly characterized. The goal of this study was to establish molecular and morphological benchmarks for tumor associated vessels (TAVs) and tumor derived endothelial cells (TDECs) during glioblastoma progression.

Methods. Using *In-Utero* Electroporation and CRISPR/Cas9 genome engineering to generate a native, immunocompetent mouse model of glioma, we characterized vascular-tumor dynamics in three dimensions during tumor progression. We employed bulk and single-cell RNA-Sequencing to elucidate the relationship between TAVs and TDECs. We confirmed our findings in a patient derived orthotopic xenograft (PDOX) model.

Results. Using a mouse model of glioma, we identified progressive alteration of vessel function and morphogenesis over time. We also showed in our mouse model that TDECs are a rare subpopulation that contributes to vessels within the tumor, albeit to a limited degree. Furthermore, transcriptional profiling demonstrates that both TAVs and TDECs are molecularly distinct, and both populations feature extensive molecular heterogeneity. Finally, the distinct molecular signatures of these heterogeneous populations are also present in human glioma.

Conclusions. Our findings show extensive endothelial heterogeneity within the tumor and tumor microenvironment and provide insights into the diverse cellular and molecular mechanisms that drive glioma vascularization and angiogenesis during tumorigenesis.

Key Points

1. Tumor-associated vessels are molecularly distinct compared to tumor derived endothelial cells.
2. Tumor-associated vessels show exceptional heterogeneity and are molecularly distinct.
3. Tumors generate their own rare endothelium, and these cells are also heterogeneous.

© The Author(s) 2020. Published by Oxford University Press on behalf of the Society for Neuro-Oncology. All rights reserved.
For permissions, please e-mail: journals.permissions@oup.com

Downloaded from https://academic.oup.com/neuro-oncology/advance-article/doi/10.1093/neuonc/noaa297/6046199 by Houston Academy of Medicine-Texas Medical Center Library user on 26 February 2021

Downloaded from https://academic.oup.com/neuro-oncology/advance-article/doi/10.1093/neuonc/noaa297/6046199 by Houston Academy of Medicine-Texas Medical Center Library user on 26 February 2021

Importance of the Study

Excessive angiogenesis and altered vessel function, both surrounding and within a tumor, are key diagnostic features in glioma. However, to date anti-angiogenic therapies have largely failed to improve patient outcomes in glioma, suggesting a deeper understanding of vessel dynamics during tumorigenesis is warranted. Here, using a combination of 3D imaging and bulk and single-cell transcriptional profiling, we defined the structural, cellular, and molecular characteristics of tumor-associated vessels (TAVs) and tumor-derived vessels (TDECs) within two animal models of glioma. Our findings reveal that TAVs and TDECs are molecularly distinct and that both cell types are highly heterogeneous. These findings create a shift in our understanding of vascular dynamics in glioma pathogenesis and suggest that a one-size-fits all approach to targeting the vasculature in glioma may not be efficacious due to the inherent molecular diversity in tumor-associated vessels, as well as tumor, derived vessels.

Glioblastoma (GBM) and high-grade glioma (HGG) represent a lethal classification of brain tumors characterized by a highly invasive and angiogenic nature. The extensive vascularization of GBM presents a significant hurdle to treating these tumors, as poorly remodeled and angiogenic vessels are considered refractory to chemotherapy and likely contribute to increased patient mortality.[1–3] To date, therapies targeting this "angiogenic switch" (eg, Avastin/bevacizumab) have failed to provide substantial clinical benefit in terms of overall patient survival.[4–6] Factors which lead to this adaptive resistance to anti-angiogenic therapy include utilizing alternative pathways to sustain tumor growth,[3,7–9] vasculogenic mimicry, tumor stem cell transdifferentiation into endothelium,[10–12] alterations in blood brain barrier (BBB) integrity, and the underlying intratumor cellular heterogeneity of GBM.[13,14] While many of these factors have been studied previously, whether morphological and cellular diversity exists in tumor-associated or tumor-derived endothelial populations, and if so what the contribution of this diversity is to tumor progression, remains unclear.[10–12] Using an endogenous mouse model of glioma,[15] we characterized tumor-associated- vessels (TAVs) and tumor-derived endothelial-cell (TDEC) populations, finding that these two endothelial cell populations are molecularly distinct. Further examination of the underlying diversity of TAVs and TDECs revealed extensive cellular heterogeneity within each of these subpopulations.

Materials and Methods

Generation of Endogenous Glioma in a Mouse Model Using In Utero Electroporation

All mouse CRISPR-IUE GBM gliomas were generated in the CD-1 IGS mouse background. In utero electroporations (IUEs) were performed as previously described.[15–17] Briefly, a plasmid containing guide RNAs targeting the tumor suppressor genes *Nf1*, *Tp53*, and *Pten* was co-electroporated along with a fluorescent reporter to label tumor cells (Supplementary Figure 1). See Supplementary Materials and Methods for more details. All mouse experiments were approved by the Baylor College of Medicine Institutional Animal Care and Use Committee.

CLARITY and Lightsheet Confocal Imaging

Adult mice were perfused via tail vein injection of 100 μL of fluorescently labeled lectin (*Lycopersicon Esculentum*) (VECTOR Laboratories, #DL-1178-1). Specimens were perfused with 1× PBS, followed by 5–7 mL of hydrogel (Logos Biosciences). Brains were drop-fixed in hydrogel solution overnight at 4 °C and cleared in electrophoretic clearing solution (Logos Biosciences, C13001) using the X-CLARITY platform (Logos Biosciences). Cleared brains were equilibrated in sRIMS at 4 °C before mounting and imaging. For more details, see Supplementary Materials and Methods.

In Vivo Miles Assay (Evans Blue Extravasation)

Mice were anesthetized and injected intravenously with 100 μL 1% Evan's blue solution (Sigma). Thirty minutes after injection, mice were euthanized and perfused with 2% PFA. Extravasation of Evans blue into the underlying brain parenchyma was determined by calculating the ratio of absorbance in nanometers per milligram of tissue. See Supplementary Materials and Methods for details.

Fluorescent Activated Cell Sorting of TAVs and TDECs

See Supplemental Materials and Methods for FACS gating conditions. Briefly, tumor tissue from dissected mouse brains was sorted using anti-mouse CD31 (Biolegend-102423), endogenous GFP signal, anti-mouse podoplanin (Biolegend-127417), anti-mouse Vegfr3/Flt4 (R&D Systems FAB743P); human: anti-human HLA-ABC (BD Bioscience-557348), anti-human CD31 (BD Bioscience-340297), anti-human podoplanin (BD Bioscience-566456), and anti-Human Vegfr3/Flt4 (R&D System-FAB3492A).

Total RNA Extraction, Library Preparation, Sequencing, and Bioinformatic Analysis

For details on mRNA isolation, library construction, and sequencing see Supplemental Materials and Methods. Briefly, total RNA was isolated from cells captured by FACS. 8 bp single index cDNA libraries were quality controlled

Neuro-Oncology

using the Standard Sensitivity NGS Fragment Analysis Kit (DNF-473–0500, Agilent formerly AATI). Equal concentrations (2 nM) of cDNA libraries were pooled and subjected to paired-end (2 × 75) sequencing of approximately 40 million reads per sample on a NextSeq.

Single Cell RNA-seq Analysis

Please see Supplementary Materials and Methods for expanded details regarding cell isolation and informatic analysis. Briefly, enriched CD31$^+$ cells isolated by Magnetic Activated Cell Sorting (MACS) were processed using the 10× Genomics Chromium single-cell gene expression platform and 9561 total cells were analyzed.

Culture of Human Glioma Cell Lines and Patient-Derived Xenografts in SCID Mice

Human glioblastoma cell lines were procured from the University of Texas MD Anderson Cancer Center, with the informed consent approved by Institutional Review Board (IRB) protocol LAB04-0001. Primary human glioma cell lines were injected into the brains of SCID mice[15] as approved by Baylor College of Medicine Institutional Animal Care and Use Committee. In some cases, neurospheres were differentiated into TDECs using described methodologies[11] and tube formation was analyzed to verify the endothelial properties of TDECs.

Results

Progressive Morphological and Functional Changes in Tumor-Associated Vessels

Previous studies described vascular development in xenografts of malignant glioma,[18] however this process has not been characterized in a mouse model that features de novo tumor growth and an intact immune system. We utilized a native mouse model of glioma that features CRISPR/Cas9-mediated disruption of *Nf1*, *p53*, and *Pten,* tumor suppressor genes commonly mutated in glioma, combined with *piggyBac* driven expression of GFP for tumor labeling[17] (Supplementary Figure 1A, B). This well-validated model[15–17] recapitulates several hallmark features of malignant glioma including histopathology, diffuse and infiltrative growth, molecular signatures, and common genetic lesions. Using this system, we examined morphological changes in TAVs via CLARITY-based tissue clearing[19] of fluorescent lectin perfused tumor-bearing brains followed by light-sheet microscopy at postnatal day 65 (P65) and P80 (Fig. 1A–F′) (Supp. Videos 1 and 2).

Analyses of vessel morphometry revealed that TAV vessel density is unchanged between P65 and P80 compared to the contralateral side of the brain (Fig. 1G). Conversely, both the branching index and the number of branch point junctions are significantly reduced in TAVs, suggesting a failure to create productive vessel networks over time (Fig. 1H, I). In addition, we examined the functional properties of tumor brain vasculature by monitoring blood brain barrier (BBB) integrity in mice bearing tumors at P65 and P80. Increased extravasation of Evans blue dye in the brain after intravenous injection was evident at P80 in the tumor tissue compared to the contralateral side (Fig. 1J-N). Collectively, these morphological and functional analyses reveal progressive changes in both tumor-associated vessel morphology and function during glioma progression, consistent with previous observations in PDOX models.[20]

Tumor Derived Endothelial Cells are Present in a Native Glioblastoma Mouse Model

In the course of our analysis, we observed that a subset of tumor-derived cells (GFP$^+$) contributed to vessels (lectin$^+$) (Fig. 1E-F′). Prior reports suggest that glioma stem cells (GSCs) contribute to the glioma vascular endothelium,[10–12] therefore we investigated whether glioma cells give rise to vessels in our model. We labeled vessels via perfusion of fluorescent lectin in P80 tumor-bearing mice and examined 3D reconstructed images for lectin-positive vessels that were labeled by the fluorescent GFP$^+$ reporter transgene. Examination of 3D reconstructed brains showed GFP$^+$ cells contributing to vessels (Fig. 2A, B). Immunohistochemistry on cryosections from P80 brains, followed by confocal imaging, identified lectin-labeled vessels that are GFP$^+$ and express the endothelial-specific marker, CD31 (Fig. 2C-D). Together, these data suggest that tumor derived cells can adopt an endothelial lineage. To quantify the extent of TDECs, we dissociated P65 and P80 tumor-bearing brains and performed FACS analysis to isolate tumor-derived endothelial cells (GFP$^+$, CD31$^+$ aka TDECs) and normal endothelial cells (GFP$^-$, CD31$^+$ aka TAVs) (Fig. 2E). Quantification revealed an average TDEC contribution of 0.36% and 0.52% of the total tumor population at P65 and P80, respectively (Fig. 2F).

To verify that FACS-isolated TDECs are tumor-derived, we performed sequencing of CD31$^+$,GFP$^+$ cells, identifying a substantial number of insertions and/or deletions (eg, in/dels) in the *Pten*, *Nf1*, and *Tp53* loci, confirming their tumor origins (Supplementary Figure 1C). To determine whether tumor cells from our mouse glioma model can generate endothelium, we generated glioma neurospheres[11] and cultured them in endothelial cell growth medium and Matrigel, which induced morphological changes that are reminiscent of tube-like structures (Fig. 2G). FACS confirmed the presence of CD31$^+$, GFP$^+$ TDECs, demonstrating that cultured gliomaspheres generate endothelial cells (Fig. 2H-I). These observations, in conjunction with our imaging data, demonstrate that our native model of glioma generates TDEC populations.

TAVs and TDECs Feature an Endothelial Signature

Having established that our mouse model contains both TAV (CD31$^+$, GFP$^-$) and TDEC (CD31$^+$, GFP$^+$) endothelial cell populations, we sought to further distinguish TAVs and TDECs from the bulk tumor. To this end, we performed RNA-sequencing of FACS isolated TAVs and TDECs from

Downloaded from https://academic.oup.com/neuro-oncology/advance-article/doi/10.1093/neuonc/noaa297/6046199 by Houston Academy of Medicine-Texas Medical Center Library user on 26 February 2021

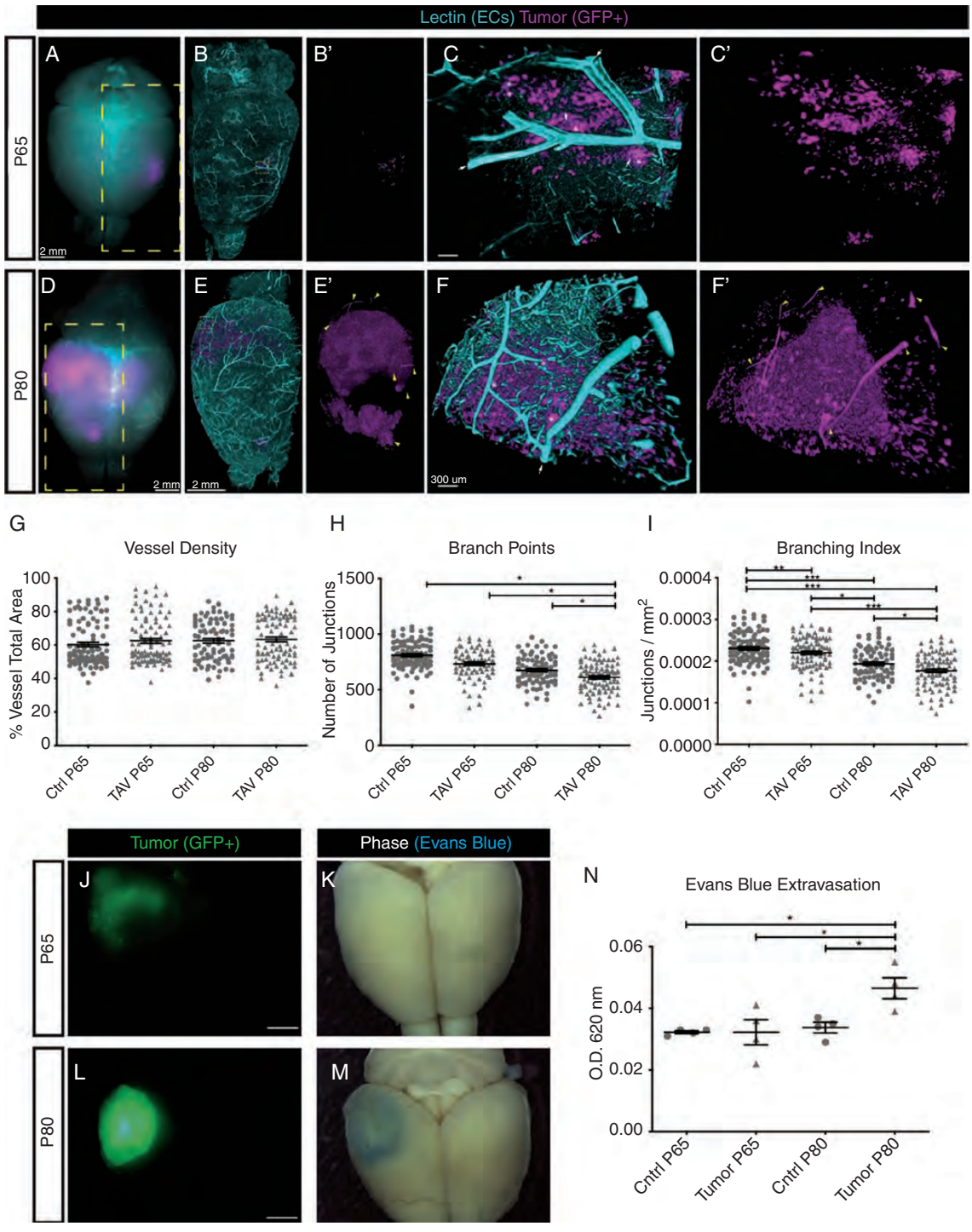

Fig. 1 Progressive morphological and functional changes in tumor-associated vessels. (A,D) Whole-mount images of an intact mouse brain at P65 (A) or P80 (D), with tumor-derived cells labeled by GFP (magenta), and vessels labeled by fluorescent lectin (teal). The yellow boxed area in (A,D), after CLARITY-based tissue clearing and lightsheet confocal imaging, is magnified and shows (B,E) vessels and tumor together or (B′,E′) tumor alone. The yellow boxed area in (B,E) is magnified and shows (C,F) vessels and tumor and (C′,F′) tumor alone. White arrows denote vessels (teal) that are associated with tumors (magenta), denoted by asterisks. Yellow carets in (E′) denote GFP$^+$ vessel-like tubes. Scale bar in A, B, B′, D, E, and E′ = 2 mM. Scale bar in C, C′, F, and F′ = 300 μm. (G-I) Quantification of vessel morphology at P65 and P80 for tumor-associated vasculature (TAV) and the contralateral non-tumor region. (J-M) Whole-mount and phase images show brain tumor progression from P65 (J, K) to P80 (L, M). Matching images of each brain following intravenous injection of Evans blue dye. (N) Quantification of Evans blue dye leak, as determined by the ratio of absorbance at $OD_{620\text{-}405\ nm}$ per milligram of tissue from the tumor area of a contralateral region from the same brain.

Downloaded from https://academic.oup.com/neuro-oncology/advance-article/doi/10.1093/neuonc/noaa297/6046199 by Houston Academy of Medicine-Texas Medical Center Library user on 26 February 2021

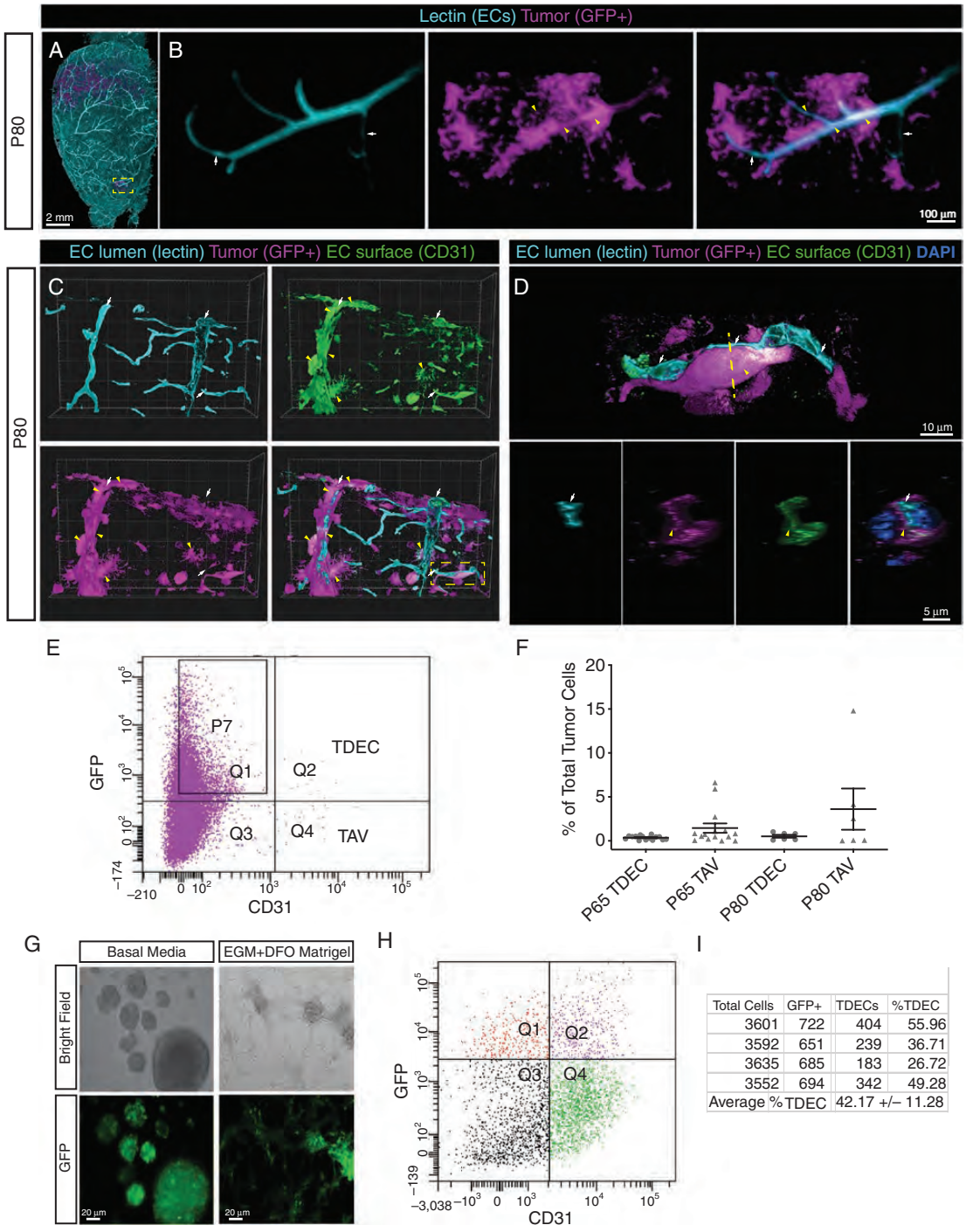

Total Cells	GFP+	TDECs	%TDEC
3601	722	404	55.96
3592	651	239	36.71
3635	685	183	26.72
3552	694	342	49.28
Average %TDEC		42.17 +/– 11.28	

Fig. 2 Tumor-derived endothelial cells are present in the native mouse model of glioma. (A) Whole mount reconstruction of a lightsheet confocal image from a P80 tumor-containing brain. The boxed area in (A) is magnified and shown in (B) with vessels (left), tumor cells (middle), and merged (right). White arrows denote vessels, yellow carets denote GFP$^+$-positive vessels. (C) Reconstructions of 40 µm thick sections from fluorescent lectin (turquoise) perfused P80 tumors (magenta) stained with CD31 (green) and DAPI (pseudo yellow) in individual and merged channels. Red arrows indicate lumen of perfused vessels, white arrows indicates tumor-derived cells (magenta) positive for CD31 (green). Boxed area is magnified in (D), showing tumor-derived cells (white arrow, magenta) enwrapping a perfused vessel (red arrow, teal). The upper panel shows a longitudinal view and the lower panel is rotated 90 degrees to show cross section view of the vessel, X-Y-Z axis is indicated. (E) Representative FACS plot from a P65 brain shows GFP$^+$ tumor-derived cells co-express the endothelial marker CD31 (TDECs). (F) Quantification of murine TAVs (CD31$^+$, GFP$^-$) and TDECs (GFP$^+$, CD31$^+$) at P65 and P80. (G) Glioma neurospheres produce tube-like structures when cultured in endothelial growth media (EGM), DFO, and grown in Matrigel. Scale bars = 20 µm. (H) Representative FACS plots of tumor neurospheres sorted for GFP$^+$ and CD31$^+$ shows co-expression of these two markers; quantification in (I).

Downloaded from https://academic.oup.com/neuro-oncology/advance-article/doi/10.1093/neuonc/noaa297/6046199 by Houston Academy of Medicine-Texas Medical Center Library user on 26 February 2021

Downloaded from https://academic.oup.com/neuro-oncology/advance-article/doi/10.1093/neuonc/noaa297/6046199 by Houston Academy of Medicine-Texas Medical Center Library user on 26 February 2021

P65 and P80 tumors, along with CD31$^+$ populations from the cortex of non-tumor bearing, age-matched mice. Comparative bioinformatics identified more than 2700 significantly differentially expressed genes between bulk tumor and the combined TAV and TDEC populations (Fig. 3A, Supplementary Table 1).

Gene Ontology (GO) analysis confirmed that TAVs and TDECs were enriched in blood vessel- and angiogenesis-related processes, while the bulk tumor displayed features of neural development (Fig. 3B, C). Analysis of individual genes within two representative GO categories, Nervous System Development and Angiogenesis, confirmed the endothelial identity of the TDEC and TAV populations (Fig. 3D). To verify that TAVs and TDECs exhibit signatures indicative of endothelial cells, we compared our results with endothelial gene expression datasets. TDEC/TAV enriched transcripts showed a strong enrichment for a VEGF-induced and angiogenic gene signature[21] compared to the bulk tumor (Fig. 3E). Additionally, we found that the signatures of TDECs and TAVs bore a striking resemblance to an established CNS dataset taken from the E14.5 (angiogenic) developing mouse brain[22] (Fig. 3F). Visualizing the angiogenic target genes (from panel "E") showed upregulation in TAVs and TDECs (Fig. 3G), reinforcing their endothelial identity.

Single-Cell Sequencing Identifies Extensive Heterogeneity Among TAVs in Glioma

To further interrogate the heterogeneity of glioma vasculature we performed single-cell RNA-sequencing on endothelial cells isolated from glioma-bearing brains. P80 brains from tumor-bearing mice were dissociated, enriched for endothelial cells, and single cell transcriptomes were generated.[23] Analysis of the cells' transcriptomes using Seurat[24] and established endothelial data sets[25,26] identified 10 distinct cell types, ranging from mural cells to EGFP$^+$ lineage tumor cells (identified by expression of GFP reporter) (Fig. 4A, Supplementary Figure 2A). Differential gene expression analysis revealed unique molecular signatures between these different clusters, as established markers of endothelium (*Glut1/Slc2a1*, *Flt1*, *Cldn5*), microglia (*Ccl12*), astrocytes (*Cspg5, Apoe, Aldoc*, *Slc1a*) and EGFP$^+$ tumor cells expressing glial, oligodendrocyte, and astrocyte markers (eg, *Rtn1, Olig1, and Fabp7*, respectively) (see Supplementary Figure 2).

Reanalysis of only the brain endothelium identified 3 separate clusters (Fig. 4C), each with a distinct molecular signature (Fig. 4B, C). While all P80 endothelial cells (ECs) were isolated by CD31$^+$ FACS, scRNA-seq failed to identity any GFP$^+$ ECs, suggesting these cells are TAVs and not TDECs. This likely reflects the rare nature of TDECs (Fig. 2E, F) and limited sequencing depth. While some pan-endothelial genes, such as *Pecam1* (encoding CD31) were expressed across P7, adult, and TAV ECs, other transcripts like the angiogenic marker *Apln* was restricted to angiogenic P7 ECs, the BBB marker *Slco1a4* (*Oatp1a4*)[27] was enriched in adult and TAV ECs, and the cell-cell junction encoding gene *Jcad* was enriched in TAVs (Fig. 4B, C and Supplementary Table 5). To understand the relationships between ECs from these three clusters, we used trajectory analysis to order the cells in pseudotime, finding that TAVs branch away from angiogenic ECs (P7 ECs) transitioning to a quiescent, homeostatic ECs (adult ECs), suggesting they represent a unique cell state (Fig. 4D). GO analysis of enriched transcripts in each of these three states showed that genes involved in cell proliferation and metabolism are enriched in P7 ECs, vesicle transport and cell to cell communication are present in adult ECs, and immune system and protein metabolism genes are enriched in TAVs (Fig. 4E). Trajectory heatmaps identified dynamic expression of genes between these states, as transcripts enriched in cell proliferation skewed toward P7 ECs, mature BBB markers are enriched in adult ECs, while ATP metabolic processes and immune genes are centered in TAVs (Fig. 4F). These data reinforce our findings that TAVs are molecularly distinct (Fig. 3) and endowed with unique metabolic and motility signatures.

Reanalysis of the P80 TAV clusters showed that the tumor endothelium features extensive heterogeneity, identifying five distinct populations (Fig. 4G) that are defined by their enrichment of distinct endothelial markers. While *Jcad*, *Spop*, and *Ctnnb1* (β-catenin, a regulator of canonical Wnt signaling and BBB integrity)[28] are expressed across all 5 clusters, clusters 2–5 are marked by the long non-coding RNA *Malat1*,[29] *Jun*, and *Arhgap31*, a critical GTPase that mediates VEGFR2 signaling.[30] Cluster 3 expressed *Matrix Gla Protein* (*Mgp*, a regulator of arteriovenous patterning),[31] *Stmn2*, and *Sema3g*, as well as the arterial marker *Gja4* (*Connexin37*). Cluster 4 was enriched for the venous marker *Nr2f2*,[32] the endothelial marker *Vwf*, *Aldh1a1*, and *Junb*, while cluster 5 was marked by expression of the chemokine receptor *CD74* and the proinflammatory chemokine *Cxcl10* (Fig. 4H, I and Supplementary Figure 2). Gene ontology analysis between these clusters demonstrates that each population is enriched for unique cellular processes (Fig. 4J).

TDEC Populations are Molecularly and Cellularly Heterogeneous

Given the extensive molecular heterogeneity within TAVs, we next sought to molecularly distinguish TAVs and TDECs. Towards this, we directly compared the TAV and TDEC transcriptomes, which revealed over 400 differentially expressed genes between the two populations (Fig. 5A). GO term analysis of these differential gene signatures revealed that genes linked to cell proliferation, cell adhesion, and cell motility, three hallmarks of angiogenesis[33] are significantly enriched in TDECs (Supplementary Table 2) (Fig. 5B). Examination of the GO category Positive Regulation of Cell Motility revealed clear upregulation of migratory genes in TDECs compared to TAVs, suggesting they are more infiltrative and angiogenic than their TAV counterparts (Fig. 5C).

To further probe the prospective TDEC heterogeneity, we segregated our existing bulk RNA-Sequencing TDEC transcriptome datasets using principle component analysis, finding that bulk TDEC datasets segregated into two populations: TDEC group 1 and group 2 (Fig. 5D). GO analysis of 1750 differentially expressed genes between the two populations revealed immune responses

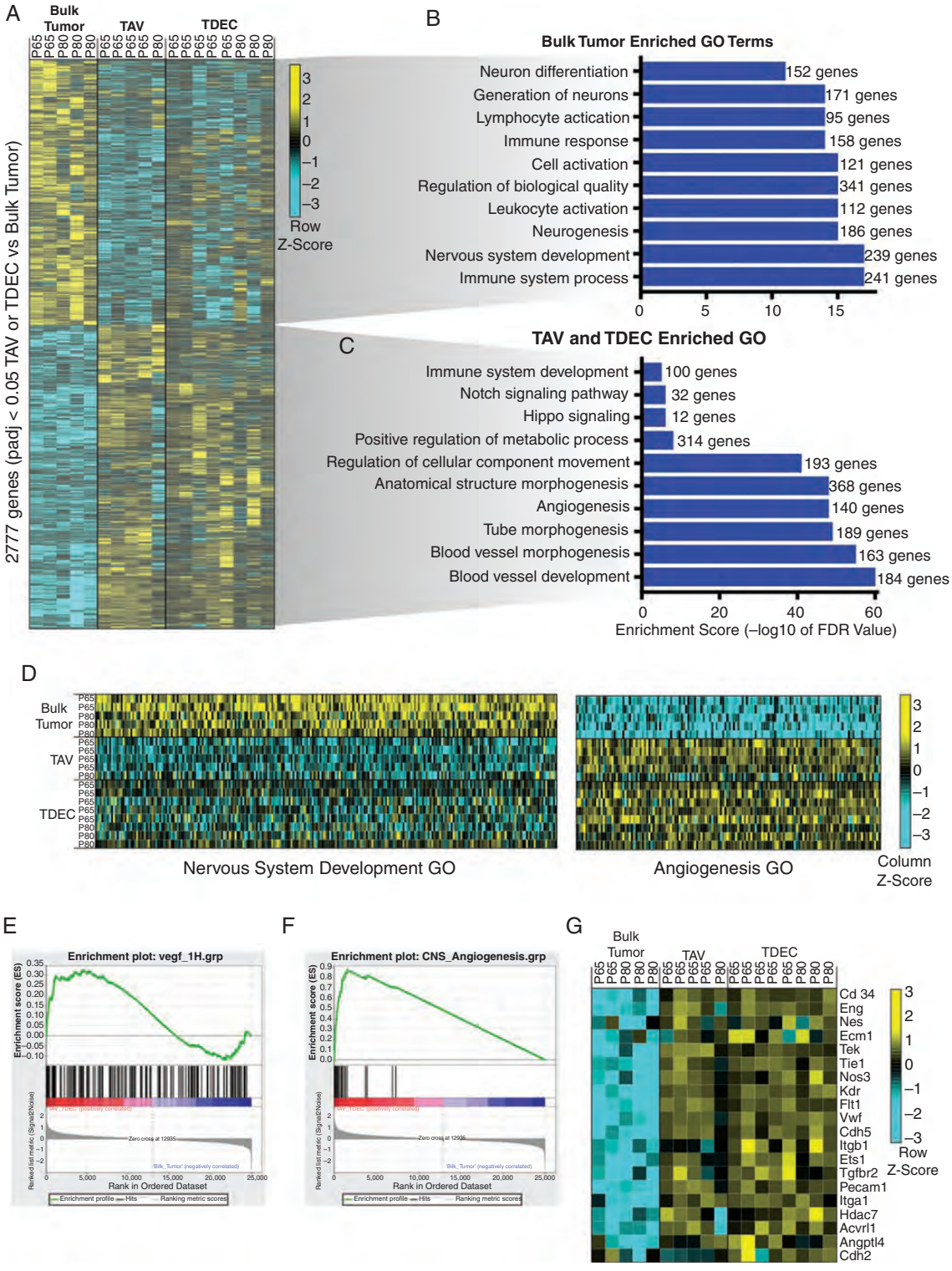

Fig. 3 Tumor-associated vasculature and tumor-derived endothelium are molecularly distinct. (A) Heatmap of differentially expressed genes detected by RNA-seq. Genes enriched are yellow, genes depleted are turquoise. Associated select gene ontology (GO) terms for genes up-regulated in either (B) bulk tumor or (C) TAV and TDEC populations. (D) Heatmap showing the individual genes for the GO categories Nervous System Development and Angiogenesis. (E) Gene Set Expression Analysis (GSEA) shows enrichment of VEGF-induced transcripts in the combined TAV and TDEC populations. (F) GSEA shows enrichment of CNS angiogenic genes in TAV and TDECs. (G) Heatmap of individual genes used for the angiogenic analysis (panel E) depicts their enrichment in the TAV and TDEC populations and depletion from bulk tumor.

Downloaded from https://academic.oup.com/neuro-oncology/advance-article/doi/10.1093/neuonc/noaa297/6046199 by Houston Academy of Medicine-Texas Medical Center Library user on 26 February 2021

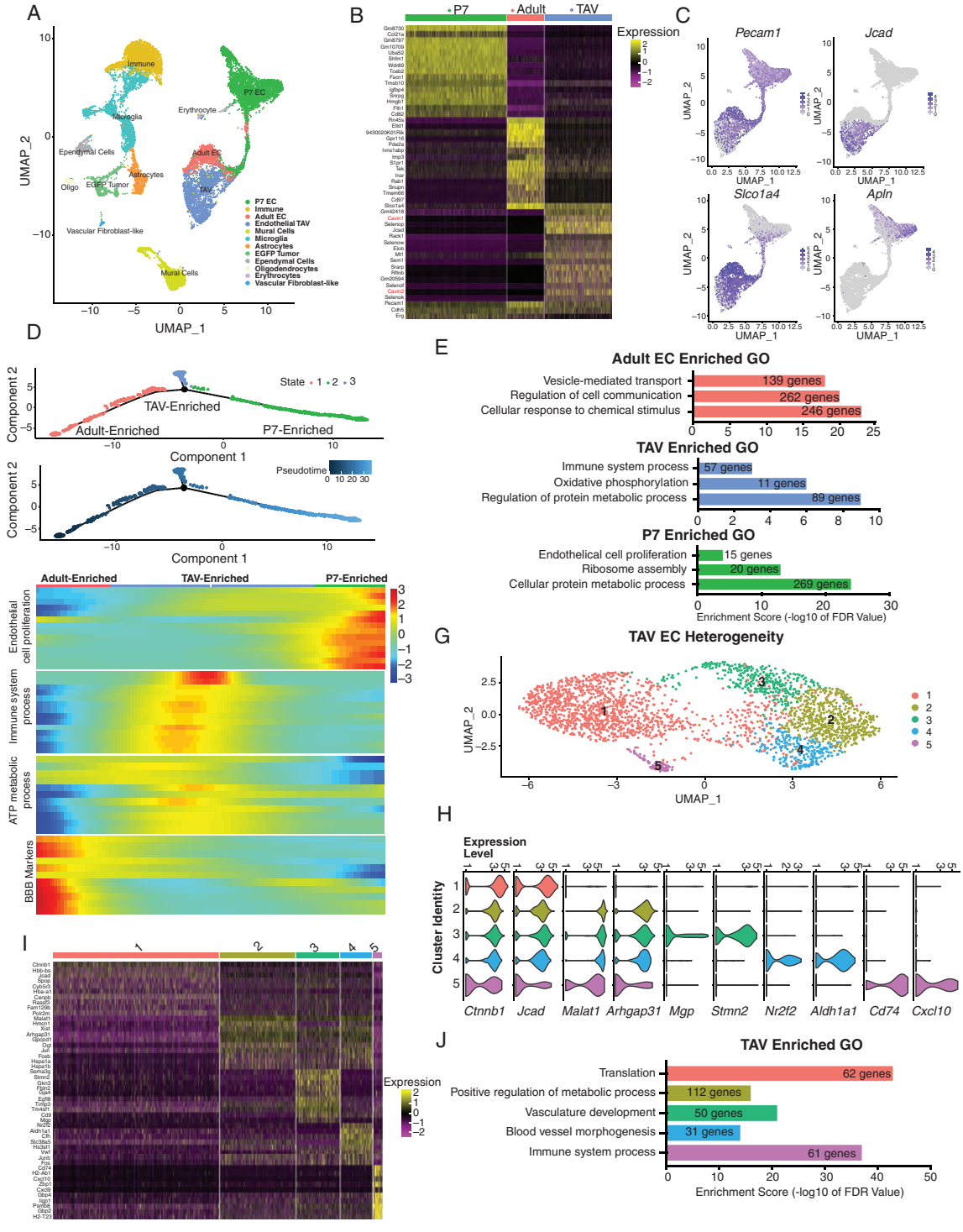

Fig. 4 TAVs display extensive cellular heterogeneity and are not simply angiogenic adult endothelium. (A) UMAP representation of scRNA-seq individual transcriptomes from wildtype P7, adult brain endothelial cells, and P80 tumor-bearing brains; each population is color-coded according to their identity (determined by cell-type specific markers). The corresponding number of cells per cluster is shown in parenthesis. (B) Heatmap showing the top 15 gene markers for each unique endothelial cell cluster. (C) Population marker expression superimposed on only the three endothelial datasets (P7, adult, and TAV). (D) Monocle trajectory analysis of P7 brain ECs, adult brain ECs, and P80 TAVs. (E) GO terms associated with enriched transcripts detected in each cell state, from panel (D). (F) Trajectory heatmap showing dynamic gene expression changes between the endothelial clusters (TAV, Adult, and P7 ECs) plotted along pseudotime as determined by Monocle trajectory analysis from panel (E). (G) UMAP representation of scRNA-seq individual transcriptomes from P80 TAVs identifies 5 unique populations, each color-coded according to their unique identity. (H) Violin plots show gene expression between the 5 different TAV clusters. (I) Heatmap of the top 10 differentially expressed genes between each population. (J) GO terms for enriched transcripts specific to each TAV population.

Downloaded from https://academic.oup.com/neuro-oncology/advance-article/doi/10.1093/neuonc/noaa297/6046199 by Houston Academy of Medicine-Texas Medical Center Library user on 26 February 2021

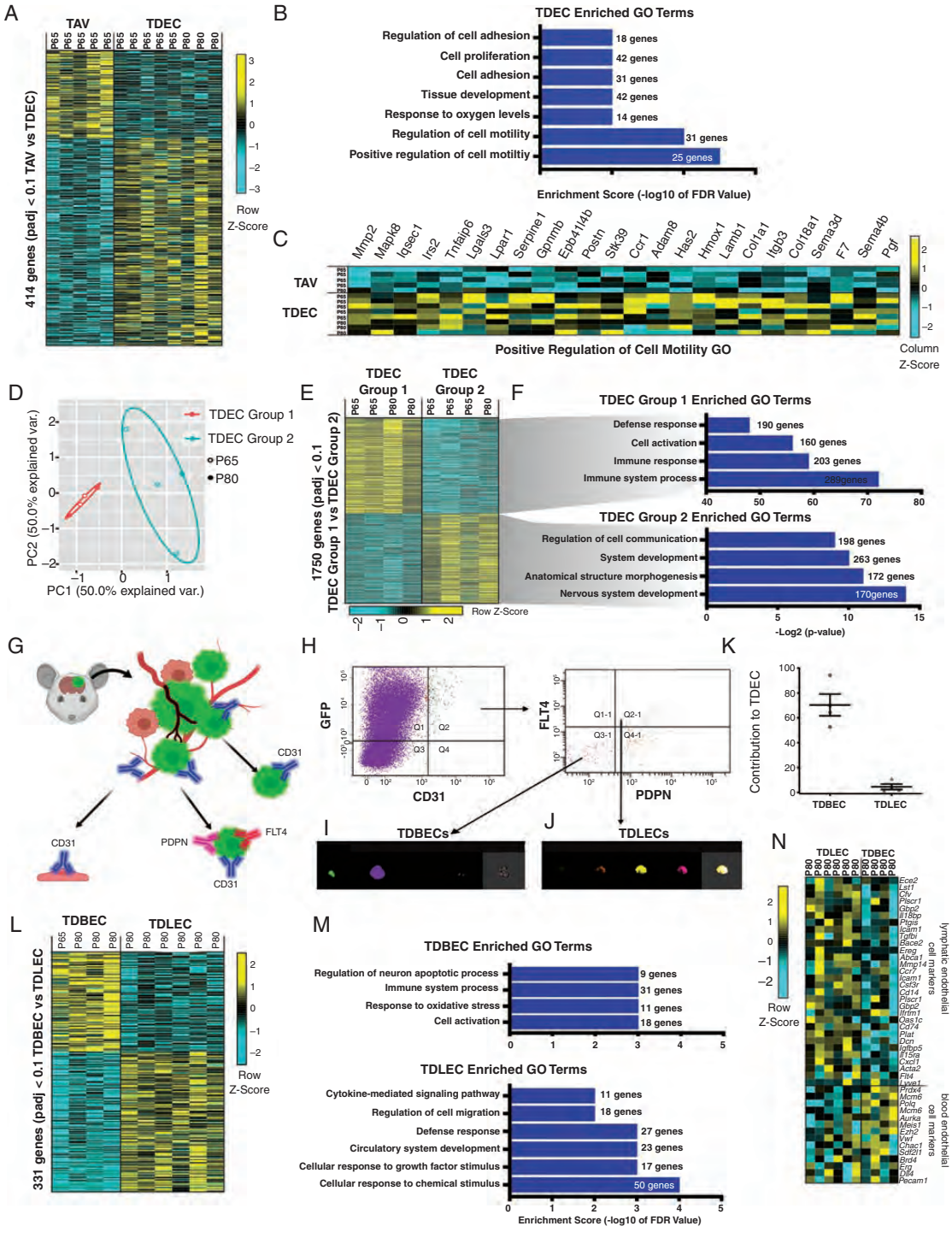

Fig. 5 Murine glioma TDECs are comprised of molecularly and cellularly unique subpopulations. (A) Heatmap of differentially expressed genes in TAVs and TDECs. Genes enriched are indicated in yellow, genes depleted are turquoise. (B) Select gene ontology (GO) terms for genes up-regulated in TDEC populations are shown. (C) Heatmap showing individual genes for the GO category Positive Regulation of Cell Migration. (D) Principal component analysis of bulk RNA-Seq shows that TDEC transcriptomes segregate into 2 groups. (E) Heatmap of differentially expressed genes detected by RNA-seq shows Group 1 (n = 4) and Group 2 (n = 4) TDECs feature distinct signatures. (F) GO terms for select genes up-regulated in TDEC Group1 and Group 2 populations. (G) Schematic illustrating the strategy for isolating TDBECs from mouse glioma. (H) Representative FACS plots demonstrating the isolation of TDBEC and TDLEC populations. (I) Representative image stream analysis demonstrating expression of GFP and CD31 in TDBECs and (J) GFP, CD31, PDNP, and FLT4 in TDLECs. (K) Quantification of TDBECs and TDLECs to the total TDEC population. (L) A heatmap of differentially expressed genes in TDBECs and TDLECs. (M) Associated select GO terms for genes up-regulated in bulk tumor, TDBEC, or TDLEC populations. (N) Heatmap of select genes upregulated in murine blood lymphatic (TDLECs) versus blood endothelial cells (TDBECs).

Downloaded from https://academic.oup.com/neuro-oncology/advance-article/doi/10.1093/neuonc/noaa297/6046199 by Houston Academy of Medicine-Texas Medical Center Library user on 26 February 2021

Downloaded from https://academic.oup.com/neuro-oncology/advance-article/doi/10.1093/neuonc/noaa297/6046199 by Houston Academy of Medicine-Texas Medical Center Library user on 26 February 2021

were significantly enriched in group 1, whereas cell-cell communication and nervous system development were upregulated in group 2 (Fig. 5E, F and Supplementary Table 2). Among the immune-related genes identified in group 1 were lymphatic cell surface markers, Podoplanin (*Pdpn*)[34] and *Flt4*,[35] suggesting that TDECs segregate into lymphatic endothelial cells (TDLECs-Group1) and blood endothelial cells (TDBECs-Group2). Next, we performed FACS on P80 native tumors, isolating GFP$^+$, CD31$^+$ endothelial cells, followed by isolation of PDPN$^+$ and FLT44$^+$ cells (Fig. 5G). This strategy revealed that TDECs can be fractionated into two subpopulations, with prospective TBECs marked by GFP$^+$, CD31$^+$, PDPN$^-$, FLT4$^-$ and prospective TDLECs marked by GFP$^+$, CD31$^+$, PDPN$^+$, FLT4$^+$ (Fig. 5G, H). Image stream analysis of verified the existence of these subpopulations, while quantification revealed TDLECs constituted a minority of TDECs (Fig. 5I-K).

RNA-Sequencing of these two TDEC subpopulations, TDBECs and TDLECs, identified more than 330 differentially expressed genes (Fig. 5L). GO analysis revealed that circulatory system, cell migration, cytokine signaling, immune and inflammatory, and interferon-alpha response genes are enriched in TDLECs (Fig. 5M).[36] Next, we used markers for blood endothelial cells (CD31$^+$, FLT4$^-$, PDPN$^-$) and lymphatic endothelium (CD31$^+$, FLT4$^+$, PDPN$^+$),[34] identifying a unique signature for TDLECs that is enriched for immune and inflammatory genes found in lymphatics, including immune cell activation marker *Icam1*, the secreted proteoglycan *Dcn*, *Tgfbi*, and MHC class II-associated invariant chain and chemokine receptor *CD74* (Fig. 5N). Collectively, these data show that glioma TDEC populations are comprised of distinct subpopulations exhibiting lymphatic and blood endothelial properties.

TDBECs and TDLECs are Present in PDOX-derived glioblastoma Tumors

To determine whether TDBEC and TDLEC populations exist in human glioma models, we intracranially injected patient-derived glioma cell lines into SCID mice (ie, PDOX model) and upon tumor formation TDBECs and TDLECs were isolated based on a combination of cell surface expression of human leukocyte antigen, CD31, PDPN, and FLT4 by FACS (Fig. 6A). FACS and image stream analysis confirmed that each of these TDEC subpopulations is present in our PDOX model of glioma (Fig. 6B-E). Subsequent RNA-sequencing on these populations yielded over 1200 differentially expressed genes (Fig. 6F). Analysis of human PDOX TDBEC and TDLEC gene ontologies revealed significant enrichment in processes that paralleled our native mouse models, such as circulatory system development and cell migration (Fig. 6G). Further analysis revealed that PDOX-derived TDBEC and TDLEC populations express a repertoire of established markers of blood endothelial cells and lymphatic endothelium, similar to their mouse counterparts (Fig. 6H; see Fig. 5N). Finally, we evaluated the expression of key genes enriched in both our murine and human TDBEC and TDLEC datasets in low- and high-grade glioma, finding significant enrichment of both signatures in high grade, but not low grade, glioma (Fig. 6I). These PDOX data, combined with observations from our native mouse model of glioma and the human TCGA data, indicate that TDLECs and TDBECs represent two unique endothelial cell populations in glioma, and suggest that while TAVs and TDECs are molecularly distinct from normal brain vasculature, as well as one another, they each feature extensive heterogeneity at a population level.

Discussion

Despite the importance of angiogenesis in cancer pathophysiology, defined functional and molecular benchmarks for vessels during glioma tumorigenesis are lacking. Utilizing both an endogenous glioma model in mice and a PDOX mouse model we characterized the morphological and functional properties of the vasculature during de novo, glioma progression. RNA-seq and scRNA-seq analysis revealed that TAVs are molecularly distinct from normal brain endothelium and that they exhibit extensive heterogeneity. Insights into the biology of TAVs has the potential to reveal new facets of the diverse microenvironment in which glioma progresses and may suggest novel therapeutic targets. For example, genes linked to the production of caveolae in the plasma membrane (eg, *Cavin-1* and *Cavin-2*) are significantly upregulated in TAVs (Supplementary Figure 3). Caveolae regulate cellular senescence and play critical roles in cell signaling. *Cavin-2* (also known as *serum deprivation response, Sdpr*) downregulates endothelial nitric-oxide synthase (eNOS) production and pathologic angiogenesis.[37,38] Interestingly, *Cavin-1 (Polymerase I and Transcript Release Factor*) is elevated in glioma and increased expression is associated with decreased survival time in patients.[39] Caveolae may control interstitial fluid pressure, which is dramatically elevated in GBM and impedes drug delivery, and these targets could represent a rationale target for future therapeutic interventions.[40]

In addition to TAVs, we also characterized the cellular and molecular properties of TDECs. While the existence of TDECs is controversial,[10–12,41,42] prior studies on this population did not define how TDECs differ from TAVs. Our analysis represents the first molecular comparison between tumor-associated and tumor-derived vascular populations in an immune-competent animal model, where tumors arise in a de novo manner, in the native brain microenvironment. Through a combination of lightsheet imaging, FACS, and transcriptomics we show that (1) that TDECs are present in a native murine model of glioma and (2) that TAV and TDEC populations are molecularly distinct cell types. Finally, it's important to note that GSC populations in PDOX models can also produce pericyte-like cells[43] and it's possible to misconstrue tumor-derived pericytes for TDECs. To resolve this, we performed immunostaining with CD13, a pericyte marker, and did not identify any GFP$^+$, CD13$^+$ cells (Supplementary Figure 4C-E). Moreover, comparative bioinformatics between pericyte gene signatures[26,44] and our TDEC transcriptional profiling data failed to reveal a significant correlation between these datasets (Supplementary Figure 4F-G). Together, these data

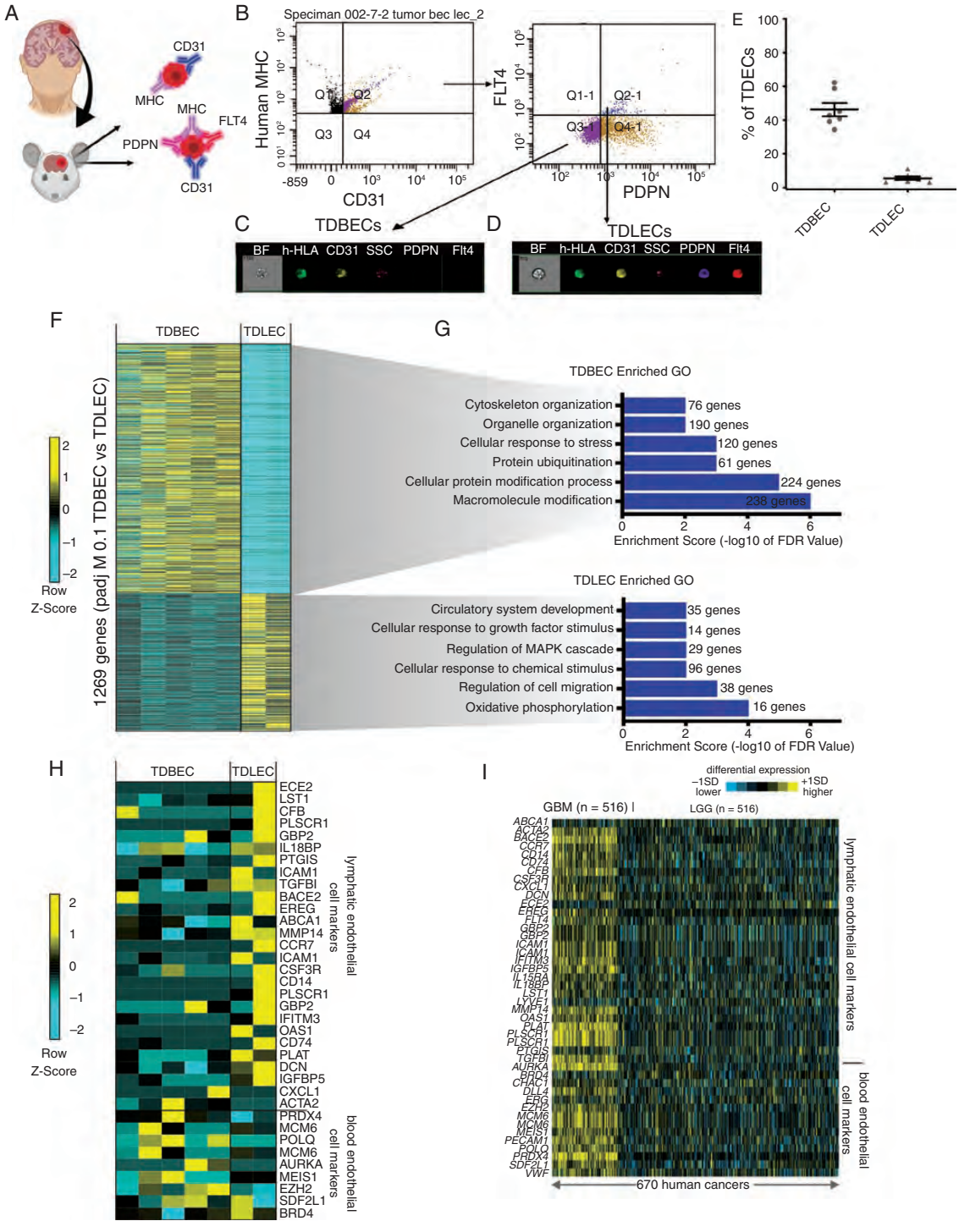

Fig. 6 TDEC heterogeneity is conserved in a human xenograft model of glioma. (A) Schematic of TDBECs and TDLECs FACS isolation from PDOX model. (B) FACS plots demonstrating isolation of human TDBEC and TDLEC cell populations from PDOX. (C) Image stream analysis demonstrating protein expression of GFP and CD31 TDBECs. (D) Image stream analysis demonstrating expression of GFP, CD31, PDNP, and FLT4 TDLECs. (E) Quantification of TDBECs and TDLECs relative to the entire TDEC population. (F) Heatmap of differentially expressed genes in PDOX TDBECs and PDOX TDLECs. (G) Select GO terms up-regulated in either human TDLEC or human TDBEC populations. (H) Heatmap depicting conserved upregulation of lymphatic endothelial transcripts in PDOX TDLECs and blood endothelial transcripts in PDOX TDBECs. (I) Heatmap showing enrichment of blood endothelial cell and lymphatic transcripts in high-grade human glioma (n = 154) compared to low-grade glioma (LGC) (n = 516) as determined by RNA-seq data from TCGA.

Downloaded from https://academic.oup.com/neuro-oncology/advance-article/doi/10.1093/neuonc/noaa297/6046199 by Houston Academy of Medicine-Texas Medical Center Library user on 26 February 2021

lend additional credence to our identification of TDEC populations.

Consistent with prior studies, we found that TDECs are a rare population, raising the question of whether such a rare population is functionally significant. Our investigations into TDEC heterogeneity provides some insight into their possible roles in tumorigenesis. Using FACS approaches with the lymphatic cell surface markers PDPN and FLT4 we found that TDECs are composed of two distinct endothelial subpopulations: TDBECs and TDLECs. Analysis of their gene expression profiles revealed that TDBECs exhibit profiles enriched for vascular development, while TDLECs possess pro-inflammatory and lymphatic signatures. Previous studies suggest that tumor-derived lymphatic cells facilitate metastasis, as primary tumor cells migrate along the lymphatic endothelium.[45] However, glioma rarely metastasizes, therefore, TDLECs may potentially play a unique role in tumor inflammation and immune cell recruitment, as they exhibit interferon-alpha and interferon-beta response signatures. Future studies on TDLECs could provide insights to the sources of inflammation in the context of a complex tumor landscape.

The unique inflammatory signatures described in TAVs, TDLECs, and TDBECs are intriguing as their potential interactions with tumor-associated macrophages and other immune populations could explain a variety of emerging immune phenotypes, including immunosuppression.[46] These data suggest that targeting specific molecular pathways controlling endothelial cell recruitment within the glioma microenvironment may be a strategy for inhibiting glioma progression or enhancing the efficacy of immunotherapy or other interventions. Moreover, we show that both TAVs and TDECs are molecularly distinct from healthy CNS endothelium, suggesting that strategies differentially targeting tumor-derived vessels, while sparing normal endothelium, may be possible.

Supplementary Material

Supplementary material is available at *Neuro-Oncology* online.

Keywords

angiogenesis | glioma | lymphangiogenesis | tumor-associated vessels (TAVs) | tumor-derived endothelial cells (TDECs)

Funding

This work was supported by grants from the Brockman Foundation (B.D. and C.J.C.), the National Cancer Institute-Cancer Therapeutic Discovery (U01-CA217842 to B.D.), the National Institutes of Health (T32-HL902332 to J.C., F31-CA243382 to E.H.H., 5T32GM088129-10 to W.D.T. 5T32HL007676-27/28 to A.M.H., NS094615 to G.R., and CA223388 to B.D.), American Heart Association (19POST34430008 to A.M.H., 19PRE34410104 to M.C.G.), Cancer Prevention Research Institute of Texas (RP150334 to B.D. and C.J.C., RP200402 to J.D.W., B.D., and C.J.C.), and a pilot award from the Baylor College of Medicine Cardiovascular Research Institute (J.D.W. and B.D.).

Authorship statement. J.C.C., J.D.W., and B.D. conceptualized the study; J.C.C. and M.C.G. designed experiments; J.C.C., M.C.G., B.L., W.D.T., E.H.H., and A.M.H. performed experiments; J.C.C., M.C.G., B.L., B.T., Y.Z., C.J.C., and J.D.W. analyzed data; J.C.C., M.C.G., J.D.W., and B.D. wrote the manuscript; M.C.G., W.D.T., A.M.H., C.J.C., J.D.W., and B.D. secured funding; All authors edited and approved the manuscript.

Conflict of interest statement. None.

References

1. Semrad TJ, O'Donnell R, Wun T, et al. Epidemiology of venous thromboembolism in 9489 patients with malignant glioma. *J Neurosurg.* 2007;106(4):601–608.
2. Jain RK, di Tomaso E, Duda DG, Loeffler JS, Sorensen AG, Batchelor TT. Angiogenesis in brain tumours. *Nat Rev Neurosci.* 2007;8(8):610–622.
3. Bergers G, Hanahan D. Modes of resistance to anti-angiogenic therapy. *Nat Rev Cancer.* 2008;8(8):592–603.
4. Kalpathy-Cramer J, Chandra V, Da X, et al. Phase II study of tivozanib, an oral VEGFR inhibitor, in patients with recurrent glioblastoma. *J Neurooncol.* 2017;131(3):603–610.
5. Xue W, Du X, Wu H, et al. Aberrant glioblastoma neovascularization patterns and their correlation with DCE-MRI-derived parameters following temozolomide and bevacizumab treatment. *Sci Rep.* 2017;7(1):13894.
6. Cha Y, Kim YJ, Lee SH, et al. Post-bevacizumab clinical outcomes and the impact of early discontinuation of bevacizumab in patients with recurrent malignant glioma. *Cancer Res Treat.* 2017;49(1):129–140.
7. Lu KV, Bergers G. Mechanisms of evasive resistance to anti-VEGF therapy in glioblastoma. *CNS Oncol.* 2013;2(1):49–65.
8. Rose SD, Aghi MK. Mechanisms of evasion to antiangiogenic therapy in glioblastoma. *Clin Neurosurg.* 2010;57:123–128.
9. Kerbel RS, Yu J, Tran J, et al. Possible mechanisms of acquired resistance to anti-angiogenic drugs: implications for the use of combination therapy approaches. *Cancer Metastasis Rev.* 2001;20(1–2):79–86.
10. Ricci-Vitiani L, Pallini R, Biffoni M, et al. Tumour vascularization via endothelial differentiation of glioblastoma stem-like cells. *Nature.* 2010;468(7325):824–828.
11. Soda Y, Marumoto T, Friedmann-Morvinski D, et al. Transdifferentiation of glioblastoma cells into vascular endothelial cells. *Proc Natl Acad Sci U S A.* 2011;108(11):4274–4280.
12. Wang R, Chadalavada K, Wilshire J, et al. Glioblastoma stem-like cells give rise to tumour endothelium. *Nature.* 2010;468(7325):829–833.

Downloaded from https://academic.oup.com/neuro-oncology/advance-article/doi/10.1093/neuonc/noaa297/6046199 by Houston Academy of Medicine-Texas Medical Center Library user on 26 February 2021

Neuro-Oncology

13. Snuderl M, Fazlollahi L, Le LP, et al. Mosaic amplification of multiple receptor tyrosine kinase genes in glioblastoma. *Cancer Cell.* 2011;20(6):810–817.
14. Eyler CE, Matsunaga H, Hovestadt V, Vantine SJ, van Galen P, Bernstein BE. Single-cell lineage analysis reveals genetic and epigenetic interplay in glioblastoma drug resistance. *Genome Biol.* 2020;21(1):174.
15. Glasgow SM, Zhu W, Stolt CC, et al. Mutual antagonism between Sox10 and NFIA regulates diversification of glial lineages and glioma subtypes. *Nat Neurosci.* 2014;17(10):1322–1329.
16. Yu K, Lin CJ, Hatcher A, et al. PIK3CA variants selectively initiate brain hyperactivity during gliomagenesis. *Nature.* 2020;578(7793):166–171.
17. John Lin CC, Yu K, Hatcher A, et al. Identification of diverse astrocyte populations and their malignant analogs. *Nat Neurosci.* 2017;20(3):396–405.
18. Lagerweij T, Dusoswa SA, Negrean A, et al. Optical clearing and fluorescence deep-tissue imaging for 3D quantitative analysis of the brain tumor microenvironment. *Angiogenesis.* 2017;20(4):533–546.
19. Chung K, Wallace J, Kim SY, et al. Structural and molecular interrogation of intact biological systems. *Nature.* 2013;497(7449):332–337.
20. Mathivet T, Bouleti C, Van Woensel M, et al. Dynamic stroma reorganization drives blood vessel dysmorphia during glioma growth. *EMBO Mol Med.* 2017;9(12):1629–1645.
21. Fish JE, Cantu Gutierrez M, Dang LT, et al. Dynamic regulation of VEGF-inducible genes by an ERK/ERG/p300 transcriptional network. *Development.* 2017;144(13):2428–2444.
22. Hupe M, Li MX, Kneitz S, et al. Gene expression profiles of brain endothelial cells during embryonic development at bulk and single-cell levels. *Sci Signal.* 2017;10(487).
23. Macosko EZ, Basu A, Satija R, et al. Highly parallel genome-wide expression profiling of individual cells using nanoliter droplets. *Cell.* 2015;161(5):1202–1214.
24. Butler A, Hoffman P, Smibert P, Papalexi E, Satija R. Integrating single-cell transcriptomic data across different conditions, technologies, and species. *Nat Biotechnol.* 2018;36(5):411–420.
25. Sabbagh MF, Heng JS, Luo C, et al. Transcriptional and epigenomic landscapes of CNS and non-CNS vascular endothelial cells. *eLife.* 2018;7.
26. Vanlandewijck M, He L, Mäe MA, et al. A molecular atlas of cell types and zonation in the brain vasculature. *Nature.* 2018;554(7693):475–480.
27. Daneman R, Zhou L, Agalliu D, Cahoy JD, Kaushal A, Barres BA. The mouse blood-brain barrier transcriptome: a new resource for understanding the development and function of brain endothelial cells. *PLoS One.* 2010;5(10):e13741.
28. Zhou Y, Wang Y, Tischfield M, et al. Canonical WNT signaling components in vascular development and barrier formation. *J Clin Invest.* 2014;124(9):3825–3846.
29. Du B, Wang J, Zang S, Mao X, Du Y. Long non-coding RNA MALAT1 suppresses the proliferation and migration of endothelial progenitor cells in deep vein thrombosis by regulating the Wnt/β-catenin pathway. *Exp Ther Med.* 2020;20(4):3138–3146.
30. Caron C, DeGeer J, Fournier P, et al. CdGAP/ARHGAP31, a Cdc42/Rac1 GTPase regulator, is critical for vascular development and VEGF-mediated angiogenesis. *Sci Rep.* 2016;6:27485.
31. Yao Y, Jumabay M, Wang A, Boström KI. Matrix Gla protein deficiency causes arteriovenous malformations in mice. *J Clin Invest.* 2011;121(8):2993–3004.
32. You LR, Lin FJ, Lee CT, DeMayo FJ, Tsai MJ, Tsai SY. Suppression of Notch signalling by the COUP-TFII transcription factor regulates vein identity. *Nature.* 2005;435(7038):98–104.
33. Potente M, Gerhardt H, Carmeliet P. Basic and therapeutic aspects of angiogenesis. *Cell.* 2011;146(6):873–887.
34. Kriehuber E, Breiteneder-Geleff S, Groeger M, et al. Isolation and characterization of dermal lymphatic and blood endothelial cells reveal stable and functionally specialized cell lineages. *J Exp Med.* 2001;194(6):797–808.
35. Mäkinen T, Veikkola T, Mustjoki S, et al. Isolated lymphatic endothelial cells transduce growth, survival and migratory signals via the VEGF-C/D receptor VEGFR-3. *EMBO J.* 2001;20(17):4762–4773.
36. Hu X, Deng Q, Ma L, et al. Meningeal lymphatic vessels regulate brain tumor drainage and immunity. *Cell Res.* 2020;30(3):229–243.
37. Boopathy GTK, Kulkarni M, Ho SY, et al. Cavin-2 regulates the activity and stability of endothelial nitric-oxide synthase (eNOS) in angiogenesis. *J Biol Chem.* 2017;292(43):17760–17776.
38. Powter EE, Coleman PR, Tran MH, et al. Caveolae control the anti-inflammatory phenotype of senescent endothelial cells. *Aging Cell.* 2015;14(1):102–111.
39. Pu W, Nassar ZD, Khabbazi S, et al. Correlation of the invasive potential of glioblastoma and expression of caveola-forming proteins caveolin-1 and CAVIN1. *J Neurooncol.* 2019;143(2):207–220.
40. Pu W, Qiu J, Nassar ZD, et al. A role for caveola-forming proteins caveolin-1 and CAVIN1 in the pro-invasive response of glioblastoma to osmotic and hydrostatic pressure. *J Cell Mol Med.* 2020;24(6):3724–3738.
41. Rodriguez FJ, Orr BA, Ligon KL, Eberhart CG. Neoplastic cells are a rare component in human glioblastoma microvasculature. *Oncotarget.* 2012;3(1):98–106.
42. Bougnaud S, Golebiewska A, Oudin A, et al. Molecular crosstalk between tumour and brain parenchyma instructs histopathological features in glioblastoma. *Oncotarget.* 2016;7(22):31955–31971.
43. Cheng L, Huang Z, Zhou W, et al. Glioblastoma stem cells generate vascular pericytes to support vessel function and tumor growth. *Cell.* 2013;153(1):139–152.
44. He L, Vanlandewijck M, Raschperger E, et al. Analysis of the brain mural cell transcriptome. *Sci Rep.* 2016;6:35108.
45. Alitalo K. The lymphatic vasculature in disease. *Nat Med.* 2011;17(11):1371–1380.
46. Takenaka MC, Gabriely G, Rothhammer V, et al. Control of tumor-associated macrophages and T cells in glioblastoma via AHR and CD39. *Nat Neurosci.* 2019;22(5):729–740.

Downloaded from https://academic.oup.com/neuro-oncology/advance-article/doi/10.1093/neuonc/noaa297/6046199 by Houston Academy of Medicine-Texas Medical Center Library user on 26 February 2021

SUPPLEMENTAL FIGURE LEGENDS

Supplemental Figure 1. Efficacy of gene editing in a CRISPR/Cas9 native mouse model of glioma. (A) A schematic detailing the generation of our native mouse model of glioma utilizing CRISPR/Cas9-mediated triple knockout of tumor suppressors, along with PiggyBac-mediated lineage tracing. In utero electroporation of E16.5 embryos with this plasmid mixture leads to fluorescently labelled brain tumors that were collected at postnatal day 65 (P65) or 80 (P80). (**B**) A detailed schematic of the three vectors comprising the glioma cocktail that are electroporated into the mouse brain at E16.5: (1) px330-*Nf1/Tp53/Pten*, (2) pGlast::PBase, (3) pB-CAG::GFP. (**C**) Next generation sequencing of TDECs pooled from they came from a sort of TDECs isolated by FACS (pooled from 3 separate animals) demonstrates the type, and frequency, of editing events present in tumor-derived endothelial cells. WT=wild type and refers to the endogenous, targeted locus in mice. Each row below WT, indicated with a number on the far left, represents different outcomes identified by bulk RNA-seq after FACS isolation of TDECs (GFP^+, $CD31^+$). Numbers to the far right indicate the number of reads per event, with the overall percentage of total reads in parentheses. Each locus targeted by the px330 glioma-inducing construct is shown. The sequence of each respective sgRNA is colored blue and italicized.

Supplemental Figure 2. Single cell profiling reveals heterogeneity among TAVs in a murine model of glioma. (**A)** UMAP representation of scRNA-seq individual transcriptomes from wildtype P7 and adult brain endothelial cells, as well as cells from P80 tumor-bearing brains, with each population color coded according to their identity (as determined by expression of established cell-type specific markers). The corresponding number of cells per cluster are shown

in parenthesis. **(B)** Heatmap showing the top 10 gene markers for each unique cluster. (C) Trajectory heatmap showing dynamic gene expression changes between the endothelial clusters (TAV, Adult, and P7 ECs) plotted along pseudotime as determined by Monocle trajectory analysis (from Figure 4E).

Supplemental Figure 3. Cavin 1 and 2 Upregulation in TAV. (**A)** Heatmap showing expression of Cavin 1/2 in bulk tumor versus TAV and TDEC from P65 and P80 mice. **(B)** UMAP of endothelial cells from TAV, Adult and P7 samples (left) and population expression of Cavin 1/2 superimposed. **(C)** Violin plots show expression levels of Cavin 1/2 in TAV, Adult and P7 EC population. **(D)** Violin plots show Cavin 1/2 gene expression between the 5 different TAV clusters.

Supplemental Figure 4. Tumor-derived cells do not give rise to pericytes or display a pericyte-like gene signature. (**A, B**) Immunohistochemical staining on thick sections from the brains of tumor-bearing mice at P80 shows that tumor-derived cells do not adopt a pericyte-like identity. Following perfusion with fluorescent lectin, which labeled the lumen of all perfused vessels (turquoise), thick sections were counter-stained with antibodies against CD13 to label pericytes (green), while tumor cells were identified by GFP signal (psuedocolored magenta). As the asterisk indicates, some tumor cells are adjacent to the vessel surface, but they do not express CD13 and a visible gap exists between the lumen, highlighted by lectin, and the tumor cells, colored in magenta. (**C, D**) A heatmap of RNA-seq reads from bulk tumor, FACS isolated TAVs (GFP-, CD31+) and TDECs (GFP+, CD31+) from the P80 mouse brain show that raw reads (log2 of the transcript count per million mapped reads, or log2PTM) do not significantly change

for pericyte markers between bulk tumor, TAV, and TDEC populations at P80. These top 50 pericyte markers come from He et al., *Scientific Reports*, 2016 and Vanlandewijck et al., *Nature*, 2018. (**D**) Enrichment of 11 specific pericyte markers from panel (**C**) are shown across all samples. Note the lack of differential expression between the samples, as the number of raw reads is consistent across each row. Applying a statistical cutoff for differential enrichment for these markers in the bulk RNA-seq data, as was done in Figures 3, 5, and 6, failed to identity any statistically significant, differentially expressed pericyte-enriched or specific genes (data not shown), unlike the clear enrichment in TAVs and TDECs for angiogenic and other vascular-related genes (Figure 3).

Supplemental Video 1. Whole mount reconstruction of the cerebrovasculature and tumor derived cells in a P65 following lightsheet imaging. Volume rendering of the cortical surface of a representative P65 mouse brain imaged by lightsheet fluorescent microscopy after perfusion with fluorescent conjugated lectin (shown in turquoise) and CLARITY tissue clearing. Tumor derived cells are labeled by endogenous EGFP (shown in magenta).

Supplemental Video 2. Whole mount reconstruction of the cerebrovasculature and tumor derived cells in a P80 following lightsheet imaging. Volume rendering of the cortical surface of a representative P80 mouse brain imaged by lightsheet fluorescent microscopy after perfusion with fluorescent conjugated lectin (shown in turquoise) and CLARITY clearing. Tumor derived cells are labeled by endogenous EGFP (shown in magenta).

Supplemental Table 1. Gene list of upregulated transcripts in Bulk Tumor, TAV and TDEC and their linked Gene Ontology terms (associated with Figure 3).

Supplemental Table 2. Gene list of upregulated transcripts in TAV, TDEC, TDEC groups 1 and 2, TDBEC, TDLEC and their linked Gene Ontology terms (associated with Figure 5).

Supplemental Table 3. Gene list of upregulated transcripts in TDBEC, TDLEC and their linked Gene Ontology terms (associated with Figure 6).

Supplemental Table 4. Gene list of upregulated transcripts in different clusters from bulk, endothelial and TAV single cell datasets and their linked Gene Ontology terms (associated with Figure 4 and Supp. Fig. 3).

Supplemental Table 5. Gene list of top 50 transcripts enriched in pericytes and known list of pericyte markers (associated with Supp. Fig. 2).

A

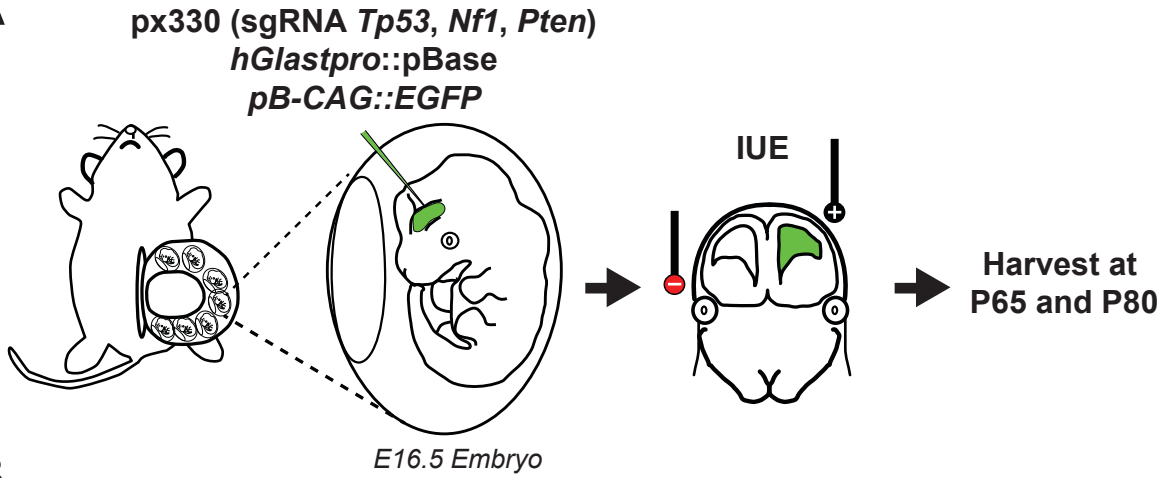

B

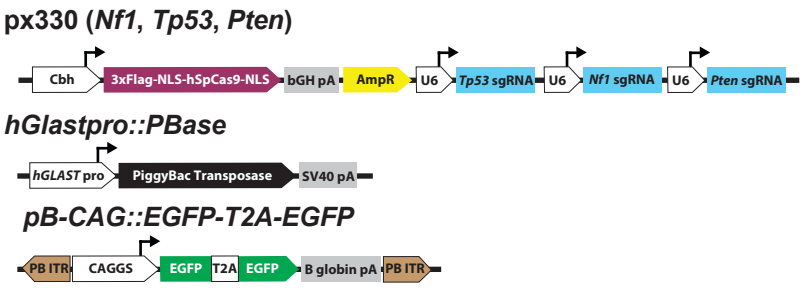

C

Murine TDEC *Nf1*

```
WT      CTGTCCTTCAACAACTCCCTCGATGTGGCGGCTCATCTGCCCTATCTCTT      997164 (32.05%)
1       CTGTCCTTCAACAACTCCCTGATG-TGGCGGCTCATCTGCCCTATCTCTT     1017731 (32.71%)
2       CTGTCCTTCAACAACTCCCTCGAATGTGGCGGCTCATCTGCCCTATCTCTT     929982 (29.89%)
3       CTGTCCTTCAACAACTCCCTCGTG-TGGCGGCTCATCTGCCCTATCTCTT      66465 (02.13%)
4       CTGTCCTTCATG------------TGGCGGCTCATCTGCCCTATCTCTT      10433 (00.33%)
5       CTGTCCTTCAACAACTCCCTC------------ATCTGCCCTATCTCTT       9212 (00.29%)
```

Murine TDEC *Pten*

```
WT      CATCATCAAAGAGATCGTTAGCAGAAACAAAAGGAGATATCAAGAGGATG     398178 (39.73%)
1       CATCATCAAAGAGATCGTTAGCAGAAACCAAAAGGAGATATCAAGAGGATG    280005 (56.50%)
2       CATCATCAAAGAGATCGTTAGCAGAAA----AGGAGATATCAAGAGGATG       7693 (01.09%)
3       CATCATCAAAGAGATCGTTAGCAGAA-----AGGAGATATCAAGAGGATG       6711 (00.95%)
4       CATCATCAAAGAGATCGTTAGCAGAAACAAAAAGGAGATATCAAGAGGATG       202 (00.03%)
5       CATCATCAAAGAGATCGTTAGCAGAA-------GAGATATCAAGAGGATG        187 (00.02%)
```

Murine TDEC *Tp53*

```
WT      TCGGATATCAGCCTCGAGCTCCCTCTGAGCCAGGAGACATTTTCAGGCTT     1531636 (38.72)
1       TCGGATATCAGCCTCGAGCTCCCTCTGAAGCCAGGAGACATTTTCAGGCTT    1019194 (58.17)
2       TCGGATATCAGCCTCGAGCTCCCTCA--GCCAGGAGACATTTTCAGGCTT       19917 (00.75%)
3       TCGGATATCAGCCTCGAGCTCCCTCTG-GCCAGGAGACATTTTCAGGCTT       13882 (00.52%)
4       TCGGATATCAGCCTCGAGCTCCCTCTG----AGGAGACATTTTCAGGCTT        4986 (00.18%)
5       TCGGATATCAGCCTCGAGCTCCCTCTGAGGCCAGGAGACATTTTCAGGCTT       3926 (00.14%)
```

Supplemental Figure 1

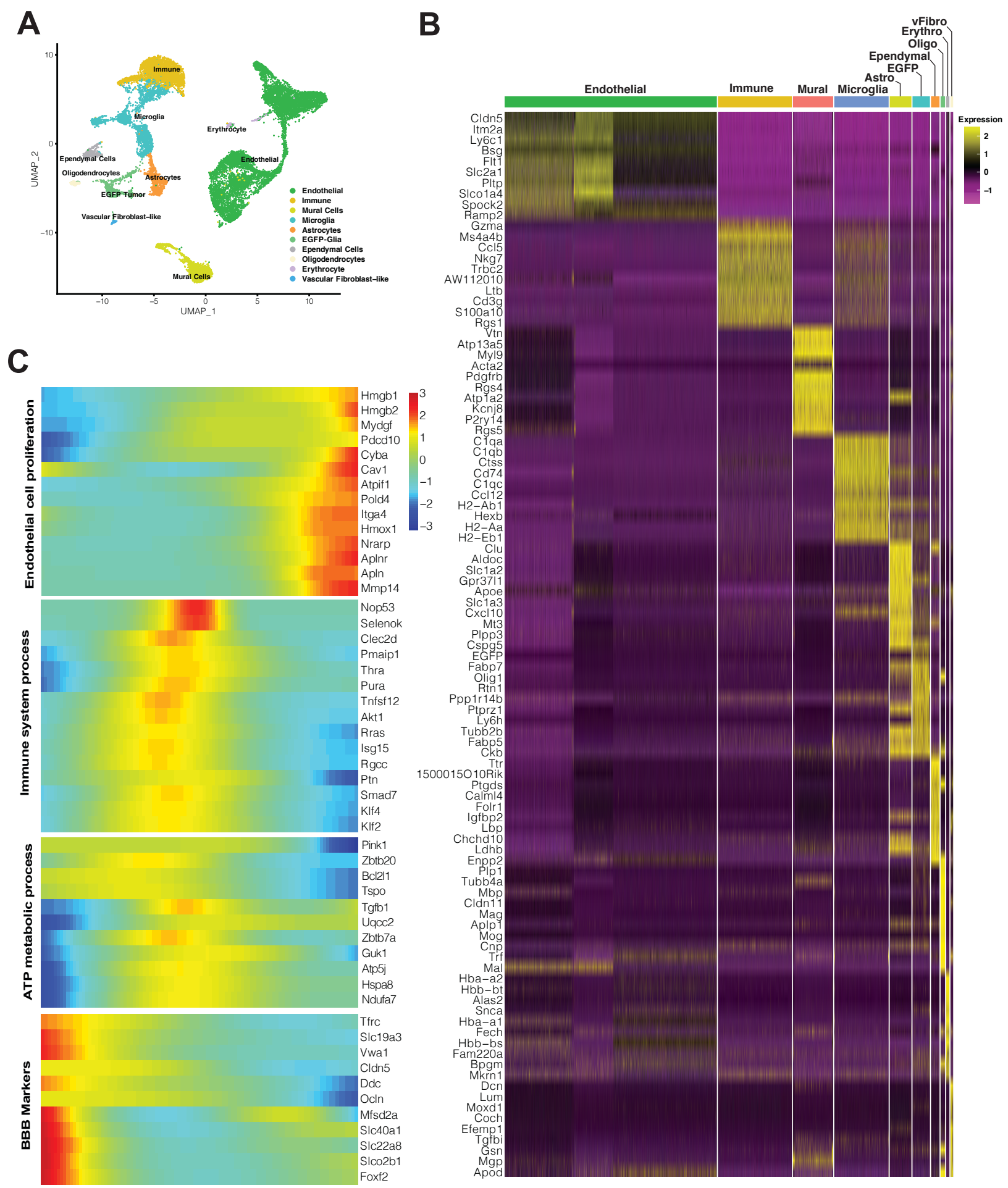

Supplemental Figure 2

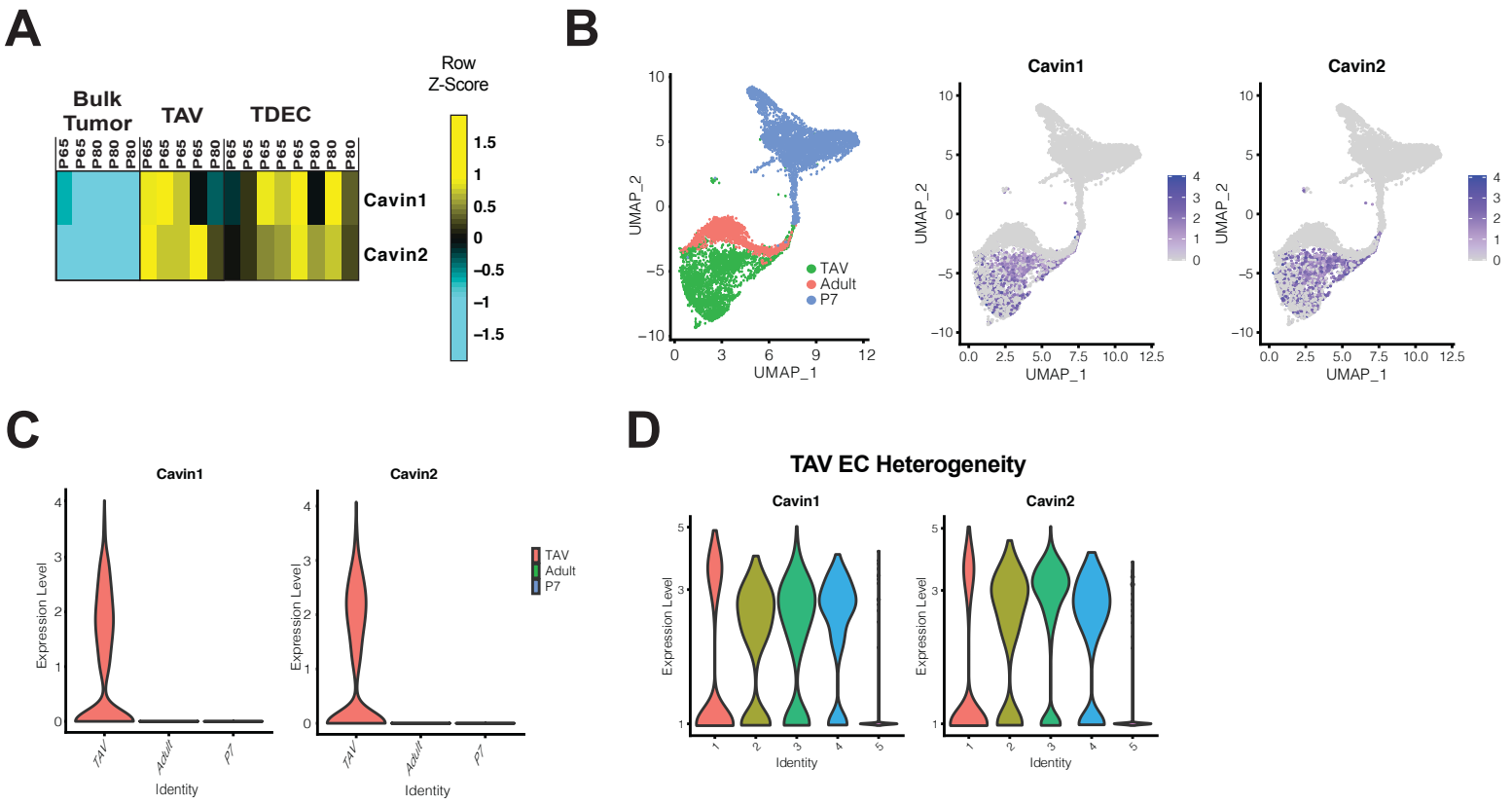

Supplemental Figure 3

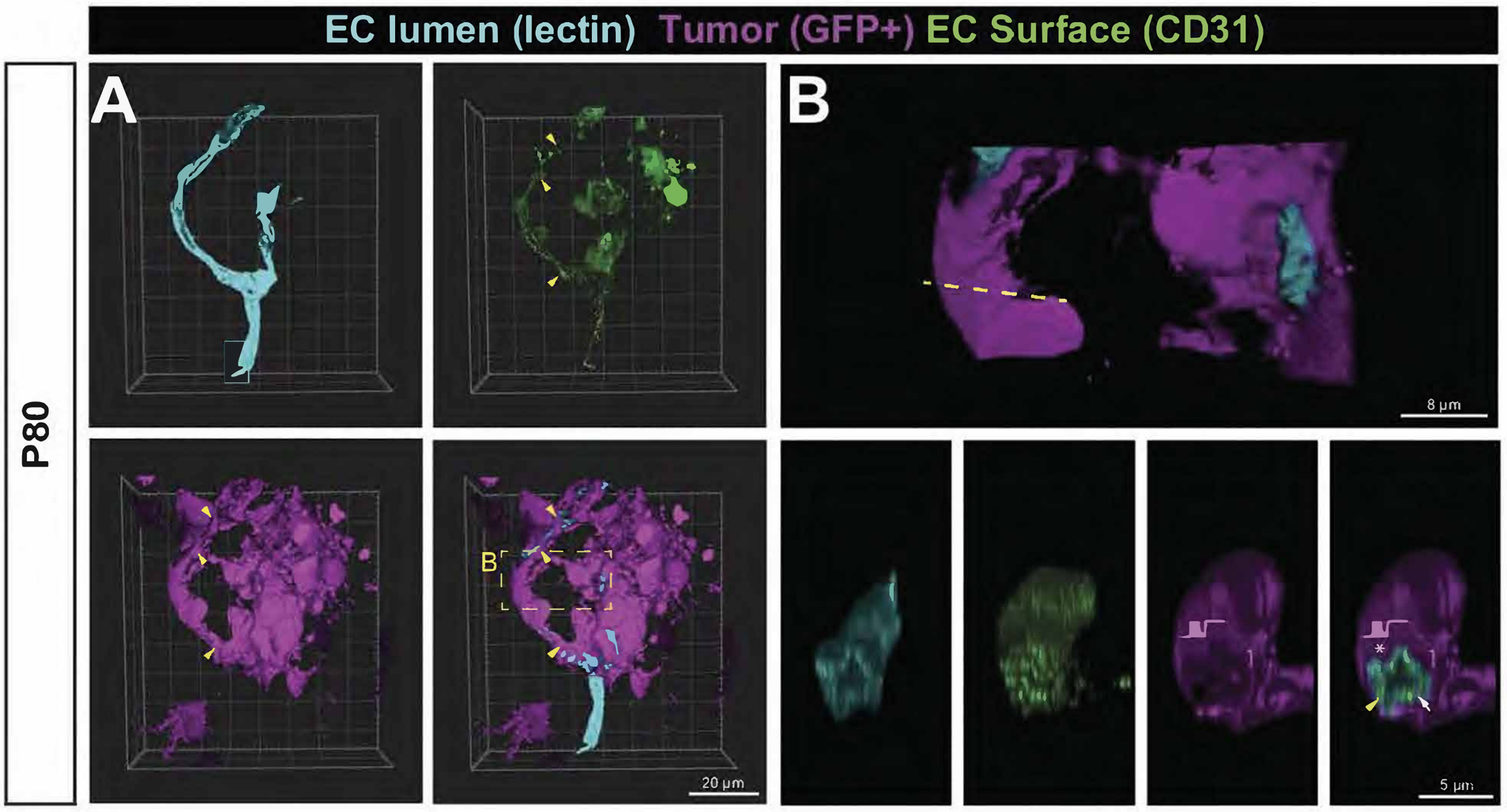

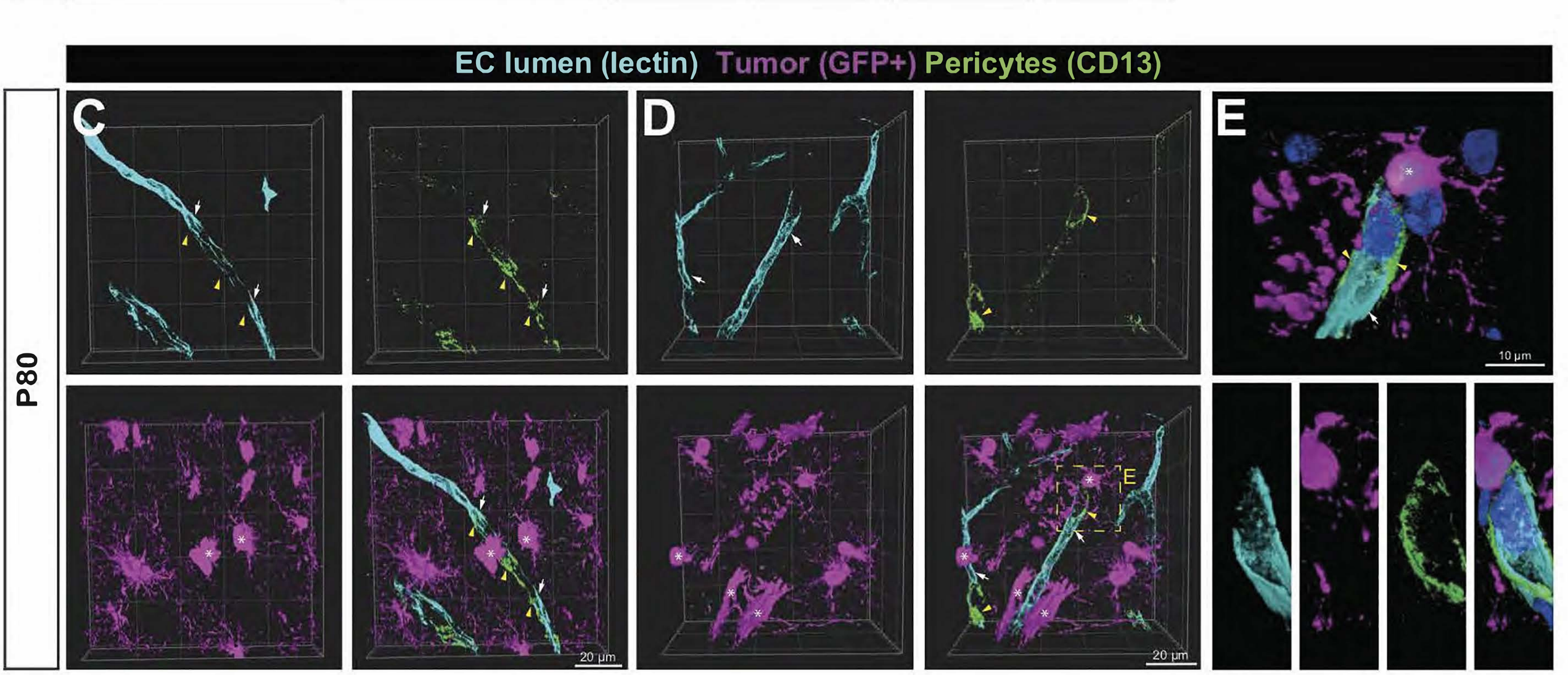

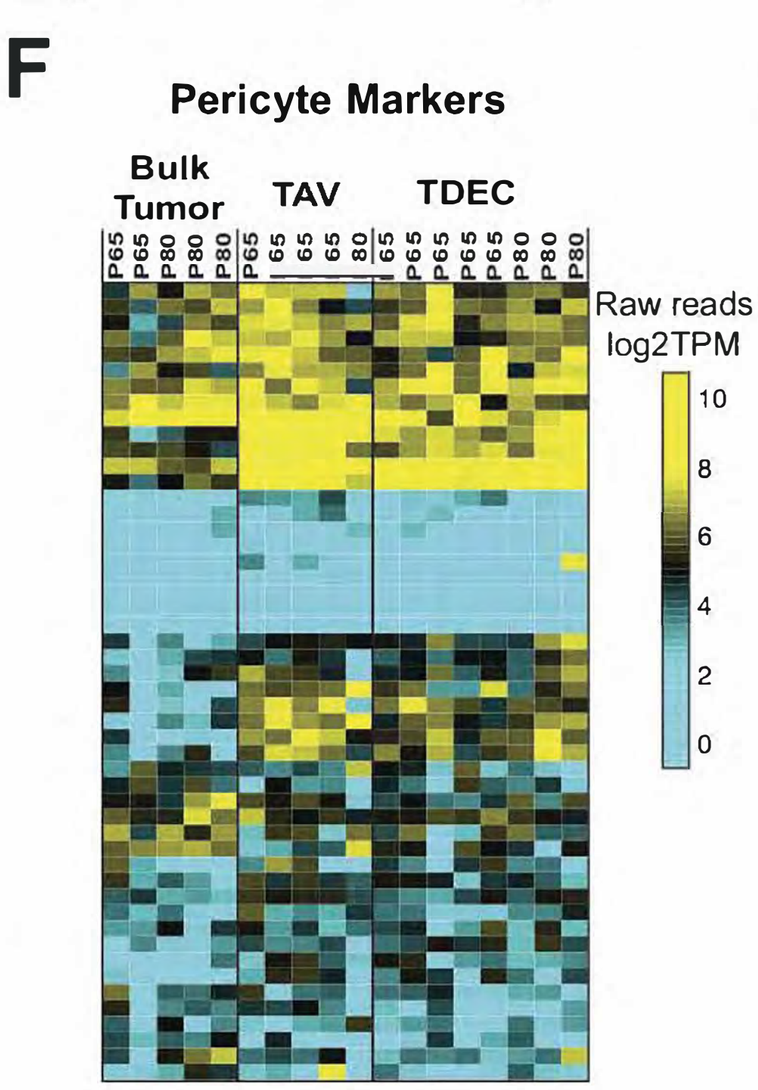

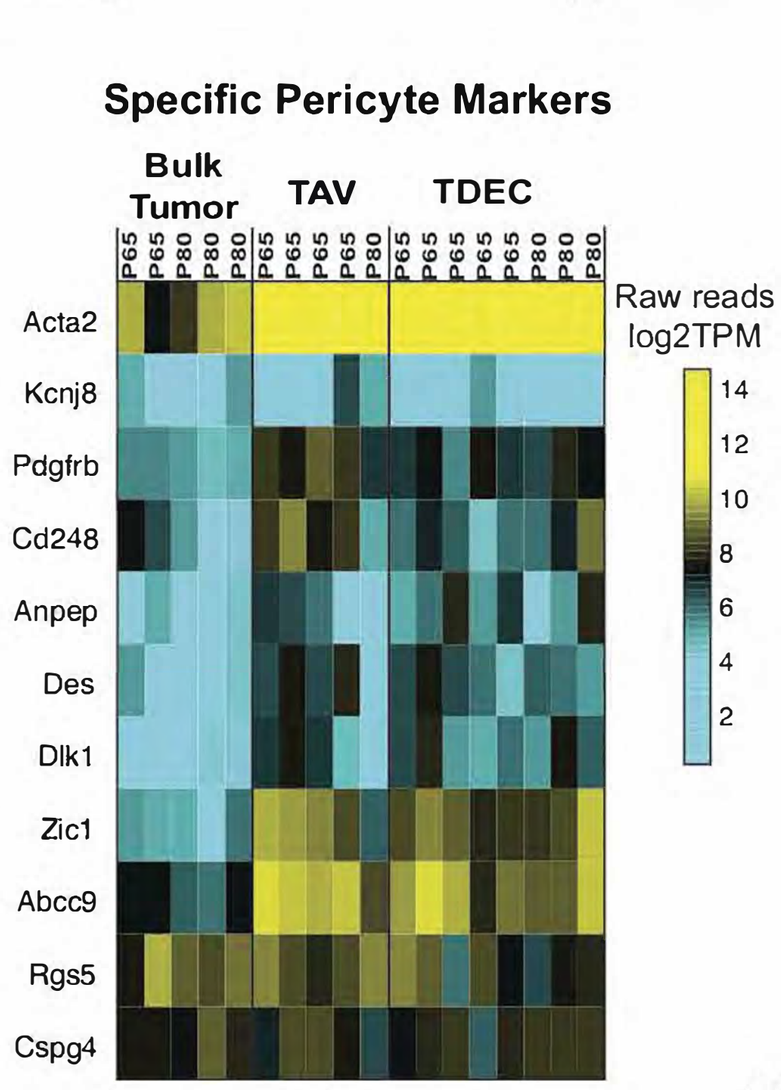

Supplemental Figure 4

Supplemental Materials and Methods

Generation of Endogenous Glioma in a Mouse Model Using In Utero Electroporation

All mouse CRISPR-IUE GBM gliomas were generated in the CD-1 IGS mouse background. In utero electroporations (IUEs) were performed as previously described [1-3]. Briefly, the uterine horns were surgically exposed in a pregnant dam at E16.5 and the embryos were injected with a DNA cocktail containing the following four plasmids: (1) a single pX330-variant [4] construct (JDW 983) encoding 3xFlag-NLS-Cas9-NLS, along with three U6 promoter cassettes upstream of validated guide RNA sequences targeting *Nf1* (GCAGATGAGCCGCCACATCGA), *Trp53* (CCTCGAGCTCCCTCTGAGCC) and *Pten* (GAGATCGTTAGCAGAAACAAA) [5] (2) a *piggyBac* (PB) helper plasmid with the glial- and astrocyte-specific promoter, *Glast*, driving expression of PB transposase (pGlast-PBase) (JDW 650) [6], and a PB cargo fluorescent reporter vector (pbCAG-GFP-T2A-GFP or pbCAG-mRFP1) (JDW 1040 or JDW 1041, respectively).

The PBase helper plasmid promotes stable integration of the cargo fluorescent reporter vector, which indelibly labels all descendant cells, allowing one to visualize tumors over time via fluorescence. Following injection of the glioma-inducing CRISPR-Cas9/PB cocktail (2.0 μg/μL pGLAST-PBase, 1.0 μg/μL all other plasmids) into the lateral ventricle of each embryo, embryos were electroporated six times at 100-ms intervals using BTW Tweezertrodes connected to a pulse generator (BTX 8300) set at 33 V and 55 ms per pulse. Voltage was applied across the entire brain to allow uptake of the constructs. The uterine horns were placed back in the cavity, and these dams developed normally, but their electroporated offspring featured malignancies postnatally, as the tumor suppressor deficient cells expanded. CRISPR-IUE tumors were harvested at postnatal day 65 (P65) and P80 from both male and female mice. All mouse

experiments were approved by the Baylor College of Medicine Institutional Animal Care and Use Committee.

Perfusion with Fluorescent Lectin

Prior to tissue collection, adult mice were injected in their tail vein with 100 µL of fluorescently-conjugated 694 nm *Lycopersicon esculentum* (tomato) lectin (Vector Laboratories, Cat. No. DL-1178). Lectin was allowed to circulate for a minimum of five minutes before tissue was harvested to allow for adequate circulation and binding of the lectin to the endothelium. Mice were then deeply anesthetized by CO_2 inhalation and the chest cavity was opened to expose the beating heart. An additional 75 µL of fluorescent lectin was injected through the left ventricle using a 31-gauge insulin syringe (BD Biosciences, Cat. No. 324911). Lectin was perfused by hand slowly over one minute and the needle was kept in place for an additional minute after injection to allow the pumping heart to circulate the dye. Afterwards, the right atrium was incised, and the animal was transcardially perfused through the left ventricle with an additional 10 mL of room temperature 1X PBS, followed by 10 mL of cold 4% PFA. The brain was then dissected from the skull and drop fixed for 48 hours, with gentle agitation, in 4% PFA at 4°C for immunohistochemistry.

CLARITY and Lightsheet Confocal Imaging

For lightsheet microscopy, animals were processed identically as described above for lectin perfusion up until the step of transcardial perfusion with PBS. After perfusion with 1x PBS, animals were perfused with 5-7 mL of hydrogel (Logos Biosciences) (4% (w/v) paraformaldehyde/ 4% (w/v) acrylamide/ 0.05% (w/v) bis-acrylamide/ 0.25% (w/v) VA-044 in

1x PBS). Brains were then dissected from the skull and drop-fixed in hydrogel solution overnight at 4°C. 24 hours later, brains were cleared in electrophoretic tissue clearing solution (Logos Biosciences, Cat. No. C13001) using the X-CLARITY platform (Logos Biosciences) (0.8 A, 37°C, 15 hours). Brains were equilibrated in sRIMS (70% w/v D-sorbitol in 1x PBS) at 4°C prior to mounting. Settings used for brain imaging: Lightsheet Z.1 microscope (Zeiss), ×5 (EC Plan Neofluar 5×/0.16) detection objective; Imaging settings: ×0.7 zoom, laser power 45v% (488 nm) and 80% (561 nm), exposure times of 100 ms; tile scan overlap 10%; Picture size: 1920 px x 1920 px; z-depth: 900 planes. Tile alignment was done with Vision4D (Version 2.12.4 ×64, Arivis AG) software. For vessel quantification: ×5 (EC Plan Neofluar 5×/0.16) detection objective; Imaging settings: ×0.8 zoom, laser power of 20v% (488 nm) and 60% (561 nm), exposure times of 40 ms; Picture size: 1920 px x 1920 px; z-depth: 280 planes. Supplemental videos were exported using Vision4D software (Version 2.12.4 x64, Arivis AG). Briefly, the 360^{o} Video Export feature was used with a Storyboard interval of five seconds per board at 1920 x1080 (16:9) video resolution and a frame rate of 30 frames per second with maximum data resolution and MPEG4 video format.

Quantification of Vascular Morphogenesis (Vessel Density, Branch Points, Branching Index)

Lightsheet confocal microscopy data were analyzed using Angiotool: a semi-automated, validated, open source software program [7]. After opening an image, AngioTool's preset parameters identifies vessel profiles, with our user-defined settings such as vessel diameter and intensity, each being set to a unit of 20 for each respective parameter. Adjustments in particles were added or removed from the segmented vascular networks based on individual image size

and signal threshold. Optimization parameters for producing consistent vascular skeletons was achieved by adjusting intensity settings per maximum intensity projection (MIP) image for each CLARITY cleared brain, which helped to detect weakly stained structures. We also spent effort assuring that careful optimization of the fill holes function for each image so true vessels were assessed. All data shown are the mean +/- the SEM. Normality of each data set was determined by visual inspection of QQ plot and a Kolmogorov-Smirnov test (given the larger sample sizes). For data that were not normally distributed (Vessel Density), a non-parametric comparison test (Kruskal-Wallis Kruskal-Wallis Multiple with Dunn's Multiple Comparison test) was employed to determine significant differences within data sets. For comparison of branch points and branching index (number of branches per mm^2), both of which were normally distributed, a one-way ANOVA and Tukey multiple comparison post-test comparing the individual means between each sample group was used to determine statistical significance.

Immunohistochemistry and Wholemount and Confocal Image Acquisition

40 micron thick sections from OCT embedded brains were left to dry at room temperature for ten minutes, then rinsed with PBS three times. Sections were then treated with blocking buffer (10% goat serum, 0.2% Triton X-100 in PBS) for 1 h at room temperature, followed by incubation overnight at 4 °C with primary antibodies diluted in blocking buffer. The following antibodies were used at the indicated dilutions: anti-CD31/PECAM (clone MEC13.3) (BD Pharmingen, Cat. No. 550274) at 1:200; anti-Aminopeptidase N/CD13 (R&D Systems, Cat No. AF2335) at 1:100. The next day primary antibody solutions were removed, and sections were washed with PBS three times for 5 min each. The slides were then incubated with secondary antibodies prepared in blocking solution (1:200) Alexa Fluor 594 Goat anti-Rat (Fisher, Cat No. A11007)

and Alexa Fluor 594 Donkey anti-Mouse IgG (Fisher, A21203) for 1 h at room temperature, washed three times in PBS, and counterstained with DAPI prepared in blocking solution (1:5,000) Sigma-Aldrich) for 10 min. The slides were then coated in Fluoromount-G™ Mounting Medium (Invitrogen, Cat. No. 00-4958-02) and coverslipped. Slides were imaged using a Zeiss LSM900 confocal microscope (Plan Apochromat 63X objective/1.40 Oil DIC M27; 405 laser power at 3.0%, 488 laser power at 0.3%, 561 laser power at 3.9%, 640 laser power at 2.8%; pinhole = 56, 28, 25 and 61 um respectively, 1024 x 1024 pixels).

In vivo Miles Assay (Evans Blue Extravasation)

Mice were anesthetized and injected intravenously in the tail vein with 100 μL of Evan's blue solution (1% (w/v) of Evans blue was prepared in normal saline then sterilized through a 0.45 μm filter prior to injection) (Sigma, Cat. No. E2129). Thirty minutes after injection, mice were euthanized and transcardially perfused with PBS then 2% PFA. Brains containing tumors were weighed and incubated in formamide solution at 56°C. 24 hours later the absorbance of the solution was measured with a spectrophotometer at 620–405 nm. Four mice per timepoint were analyzed. Extravasation of Evans blue into the underlying brain parenchyma was determined by calculating the ratio of absorbance in nanometers per milligram of tissue collected. Four mice per time point were analyzed. Analysis with a visual inspection of a QQ plot, as well as a Shapiro-Wilk test (due to the small sample size) determined that the data were normally distributed. A one-way ANOVA (Tukey multiple comparison post-test) was used to determine significance between the sample groups.

Fluorescent Activated Cell Sorting of Murine Endothelial Subpopulations

Unique subpopulations of cells from the brain were isolated by FACS, as previously published [8,9]. Briefly, tumor tissue from a dissected mouse brain was dissociation with papain (10 units/ml) (Sigma Aldrich, Cat. No. P3125) with DNase I (20 units/ml) (NEB, Cat. No. M0303S) at 37°C for twenty minutes with gentle agitation. DMEM+F12 media [Thermoscientific, Cat. No. 12634010) supplemented with 10% FBS (Thermoscientific, Cat. No. 26140079] was added for neutralization, and the suspension was centrifuged at 2000 RCF for five minutes at room temperature. The pellet was resuspended in FACS buffer (Leibowitz medium (Thermoscientific, Cat. No. 21083027), supplemented with 1 mg/ml BSA (Thermoscientific, Cat. No. B14), 10 mM HEPES pH 7.05, penicillin–streptomycin (Thermoscientific, Cat. No. 15140148) and the cells were incubated with primary antibodies for 45 minutes. Primary antibodies used included anti-mouse CD31 (0.2 μg/ml) (Biolegend-102423), anti-mouse podoplanin (0.2 μg/ml) (Biolegend-127417), anti-mouse Vegfr3/Flt4 (0.2 μg/ml) (R&D Systems, Cat. No. FAB743P). Cells were then washed with PBS and suspended in FACS buffer (described above). Primary antibodies were incubated concurrently.

Acquisition and analysis were performed on a FACSAria II (BD Biosciences) using FACSDIVA software (BD Biosciences). Laser lines utilized were a Violet (407 nm) laser (450/50 nm emission filter), Blue (488 nm) laser (530/30 nm emission filter), Yellow-Green (561 nm) laser (585/15 nm emission filter), and Red (638 nm) laser (760/60nm emission filter), in addition to Forward Scatter (FSC), Forward Scatter PMT, and Side Scatter (SSC). A 100-μm/20-p.s.i. nozzle setting was utilized to accommodate for average approximate tumor cell size and viability. The gating tree was set as follows: FSC/SSC (which represents the proportion of cells in the light scatter based on size and intracellular granularity) to B: FSC/pulse width (excludes events that could represent more than 1 cell and was used to exclude potential doublets) to C:

FSC/GFP positive (to identify tumor-derived cells) D: GFP/CD31-BV421 (identifies selective subsets of tumor-derived endothelium versus tumor microenvironment) or E: biexponential VEGFR3-PE/PDPN-APC-Cy7 (selects for lymphatic-like, aka TDLEC, and blood-like, aka TDBEC, subsets of endothelium). A total of 50,000 cells were analyzed; however, further cellular events were captured post-analysis in order to generate enough genetic material for sequencing. Initial SSC and FSC criterion were set utilizing fluorescent negative cells from the contralateral side of the brain. Subsequent mono-fluorescent parameters to establish further gating were determined by single color excitation channels utilizing positive controls. Cells that were positive for internal lineage dependent expression of EGFP and appropriate cell surface markers were sorted into a 1.5-ml tube containing 1x PBS for downstream analysis.

RNA-Seq of murine bulk tumor, TAVs, and TDECs

For P65 brains, an average of 50,311 GFP^+ tumor cells were isolated, and of those 153 were TDECs (AVG=0.364%, STD=0.2195). From these same brains, roughly 410 cells were TAVs (AVG=1.45%, STD=2.006) (n=15). From the P80 brain, approximately 66,088 GFP^+ tumor cells on were isolated on average (from 2-5 million sorting events), with 482 TDECs (AVG=0.5177%, STDEV=0.3766) and 393 TAVs (AVG=3.612%, STDEV=5.239) per brain (n=6). Cells were captured via FACS from bulk tumor, TAVs, and TDECs and total RNA was isolated using Trizol (Thermoscientific, Cat. No. 15596018) and the RNeasy Micro Kit (Qiagen, Cat. No. 74004). RNA quality was confirmed on a 12-Capillary Fragment Analyzer using the High Sensitivity RNA Analysis Kit (Agilent formerly AATI, Cat. No. DNF-472-0500). Approximately 5 ng of total RNA was used for cDNA library construction using the Trio RNA-Seq System (0507-96, NuGEN). 8-bp single index libraries were quality controlled using the

Standard Sensitivity NGS Fragment Analysis Kit (Agilent formerly AATI, Cat. No. DNF-473-0500,). Samples were quantified with Quant-iT dsDNA Assay Kit, high sensitivity (Thermo Fisher, Cat. No. Q33120,) and equal concentrations (2 nM) of libraries were pooled, diluted and denatured according to the manufacture's protocol. Libraries were subjected to paired-end (2x75) sequencing of approximately 40 million reads per sample using the High Output v2 kit (Illumina, Cat. No. FC-404-2002) on a NextSeq500.

Ultra-Low Input Bulk RNA-Seq of Murine and Human PDX Tumor-Derived Endothelial Subpopulations

Rare, tumor-derived endothelial cells—TDLECs and TDBECs—from both our native CRISPR/Cas9 murine model and human PDOX mice, as well as PDOX bulk tumor cells, were isolated by FACS and were collected in 1x PBS (Thermoscientific, Cat. No. 10010023). Total RNA was extracted using Trizol (Thermoscientific, Cat. No. 15596018) and the RNeasy Micro Kit (Cat. No. 74004, QIAGEN). Approximately 250 pg of total RNA was isolated from 2,000 murine or human PDX-derived TDLECs and TDBECs, as well as bulk tumor PDX-derived cells. cDNA was synthesized using the SMART-Seq Ultra Low Input RNA Kit (Takara, Cat. No. 634889). cDNA concentration and quality were determined using the High Sensitivity NGS Fragment Analysis Kit (Agilent, Cat. No. DNF-474-0500) on a 12-Capillary Fragment Analyzer (Advanced Analytical Technologies Inc.). Quantification of cDNA was confirmed using the Quant-iT dsDNA Assay Kit, high sensitivity (Thermo Fisher, Cat. No. Q33120). Sequencing libraries were produced using the Nextera XT DNA Library Kit (Illumina, Cat. No. FC-131-1024) with 50 pg of cDNA input for tagmentation and ligation at ½ the manufacture recommended volumes. The resulting dual indexed Illumina sequencing libraries were validated

using the Standard Sensitivity NGS Fragment Analysis Kit (DNF-473-0500, Agilent formerly AATI) and subjected to paired-end (2x75) sequencing at a depth of approximately 40 million reads per sample using a High Output v2 kit, (Illumina, Cat. No. FC-404-2002) on a NextSeq500, according to the manufacture's protocol.

Statistical Analysis and Bioinformatics Processing for Bulk RNA-seq Data

Demultiplexed FASTQ files from each flow cell lane were downloaded and merged from BaseSpace. Quality control of each sample was assessed using fastQC (v0.10.1) and MultiQC (v0.9) [10]. Reads were aligned to the mouse reference genome mm10 assembly using Salmon [11]. Transcript level quantification was then analyzed using DESeq2 (v1.20.0) [12] and imported using tximport (v1.14.2) [13]. DESeq2 was used for read count normalization in RStudio (v3.5.2) (http://www.rstudio.com/). DESeq2 was used to perform differential gene expression analysis of Bulk, TDEC and TAV populations. Differentially expressed genes were defined as those transcripts with an expression log2fold-change >0.5 and a Benjamini-Hochberg adjusted p-value (q-value) of less than 0.05. TAV versus TDEC (and TDEC group 1 versus 2) differentially expressed genes were defined as those transcripts with an expression log2fold-chang >0.5 and q-value <0.1. Enrichment analysis of selected genes in TAV, TDEC and Bulk Tumor was done using Gene Set Enrichment Analysis (GSEA) [23,24]. DESeq2 was also used to identity subpopulation specific gene signatures for murine TDLECs versus TDBECs, as well as human TDLECs versus TDBECs (log2fold-chang >0.5 and q-value <0.1). These differentially expressed genes were then used to identity unique biological processes present in each cell type via Gene Ontology analysis using ShinyGO [14].

Magnetic Activated Cell Sorting for Murine Single Cell RNA-Sequencing

Processing of tumor tissue for MACS was virtually identical to tissue preparation for FACS until the step of papain neutralization. At this point, the cell suspension was pelleted, the pellet was washed two times with PBS and then resuspended in 180 μL MACS PEB buffer (phosphate-buffered saline (PBS), pH 7.2, 0.5% bovine serum albumin (BSA), and 2 mM EDTA by diluting MACS BSA Stock Solution (Miltenyi Biotec, Cat. No. 130-091-376) 1:20 with autoMACS Rinsing Solution (Miltenyi Biotec, Cat. No. 130-091-222). The cell suspension was then incubated for 15 minutes with 20 μL of anti-CD31 MicroBeads (Miltenyibiotec, Cat. No. 130-097-418) at 4°C. Cells were then washed with 1 mL of PEB buffer, centrifuged at 300 xg for 5 minutes, and applied to an MS Column (Miltenyi Biotec, Cat. No. 130-042-201) on a magnetic stand. Cells were collected after three consecutive washes with 0.5 mL of PEB. These cells were then pelleted at 300 xg for 10 minutes at 4°C, then resuspended in 1x PBS at a concentration of 50,000 cells per 50 μL in a total of 50 μL with a viability ≥ 90% and then used for downstream applications (see below).

Single Cell RNA-Sequencing of Murine Brain Cells

Using the Single Cell Genomics Core at Baylor College of Medicine, single cells were isolated using the10x Genomics Chromium Controller Instrument within a Chromium Next GEM Chip G (10X Genomics, Cat. No. PN-1000120) platform, and the resulting libraries were created with a Chromium Next GEM Single 3' GEM, Library and Gel Bead Kit v3.1 (10X Genomics, Cat. No. PN-1000121). Samples were then indexed using a Chromium i7 Multiplex Kit (10X Genomics, PN-120262). 9,728 total cells were analyzed at an average sequencing saturation of 60.1%. Raw sequencing data were handled using the 10x Genomics Cell Ranger software

(www.10xgenomics.com). Fastq files were mapped to the mm10 genome, and gene counts were quantified using the Cellranger count function. For bulk brain single cell, there was an average of 12,845 reads per cell, and detected an average of 1,028 genes per cell. For endothelial enriched single cell sequencing, there was an average of 44,884 reads per cell and detected an average 774 genes per cell. P7 and adult brain single cell datasets were imported from previously published studies [15,16].

Statistical Analysis and Bioinformatics Processing for scRNA-seq Data

Expression counts were imported into Seurat (version 3.2.0, https://satijalab.org/seurat/) for log normalization. Cells with a percentage of mitochondrial reads above 20% and with less than 200 features were filtered out. Batch effects were corrected by regressing out the number of mitochondrial read percentage using the vars.to.regress and ScaleData function. Next, principal component analysis (PCA) was performed and significant principal components were used for graph-based clustering. UMAP was used for 2-dimensional visualization [17]. Differential expression of genes per cluster was performed using the Wilcoxon rank sum test (FindMarkers function default). For pseudotemporal analysis, normalized data from endothelial cells were passed from Seurat to Monocle2 [18-20]. The Monocle2 BEAM statistical test was utilized to determine genes changing in a pseudotemporal manner. Lastly, P7 and adult brain endothelial cells, and then TAVs were reanalyzed using Seurat. Genes differentially enriched in each cluster and were then used to identity unique biological processes present in each cell type via Gene Ontology analysis using ShinyGO [14].

All bulk RNA-seq and scRNA-seq datasets have been uploaded to the Gene Expression Omnibus (GEO accession: GSE158700). The two previously published brain EC datasets used were GSE111839 (P7) [16] and GSE98816 (adult) [15].

Cell Culture of Human Glioma

Glioblastoma cell lines (NA06, 4-23, 7-11) were isolated from patients with glioblastoma at the University of Texas MD Anderson Cancer Center (Houston, Texas). The diagnosis of glioblastoma was established by histological examination, according to the WHO (World Health Organization) classification. Samples derived from patients were obtained with the informed consent of patients under an ethically approved Institutional Review Board (IRB) protocol LAB04-0001 (chaired by F.F. Lang). Tumor specimens were resuspended in a 1:1 mixture of Dulbecco's modified Eagle's medium/ Ham's F-12 medium (DMEM/F12) (ThermoFisher) supplemented with B27 (1x, ThermoFisher), bFGF (20 ng/ml, Peprotech), and EGF (20 ng/mL, Peprotech). Cells were cultured as neurospheres using DMEM/F-12, supplemented with B27 and N12 (ThermoFisher), 10 ng/ml EGF, and 10 ng/ml bFGF. Neurospheres were incubated using standard methods [21] and passaged every 5-7 days based on sphere size.

Generation of Patient Derived Orthotopic Xenografts in SCID Mice

Six-week-old SCID male mice (Taconic) were used for human GBM cell line transplantation as previously described (15). Glioblastoma cell lines (NA06, 4-23 and 7-11) Briefly, 50,000 of these primary human GBM cells (from lines NA06, 4-23, and 7-11) were injected into each mouse brain, at the location of the -1.8 mm AP, +1.5 mm right ML, -1.4 mm deep DV from

Bregma. Eight weeks after transplantation of these patient derived, xenografted (aka PDX) GBM cells, mice were humanely euthanized and GBM cells collected via FACS (as described below).

FACS of Human Glioma Stem Cell Derivatives from PDX Mouse Models

Mouse brains were processed exactly as described above, except the following antibodies were used to isolate unique human Glioma Stem Cell-derived (GSC) cell populations: anti human HLA-ABC (0.2 ug/ml) (BD Bioscience, Cat. No. 557348), anti-human CD31 (0.2 ug/ml) (BD Bioscience, Cat. No. 340297), anti-human podoplanin (0.2 ug/ml) (BD Bioscience, Cat. No. 566456), anti-Human Vegfr3/Flt4 (0.2 ug/ml) (R&D System, Cat. No. FAB3492A). Cells were collected in 1x PBS then used in downstream applications.

FACS Image Stream Analysis

Briefly, FACS stream image analysis was performed using an Amnis ImageStreamX Mark II. This instrument assesses cellular input and produces multiple high-resolution images of every cell directly in sheath flow, sensitivity exceeding conventional flow cytometers. 20X magnified images were captured using 405 nm (Violet), 488 nm (Blue), 561 nm (Yellow-Green), and 642 (Red) nm lasers, as well as Side Scatter and Brightfield channels.

In vitro Tube Formation Assays using Murine Glioma Neurosphere-Derived Endothelial Cells

Murine-derived glioma neurospheres were differentiated into TDECs in vitro using previously described methodologies [22]. Briefly, 5,000 murine GFP^+ glioma cells were isolated by FACS and then cultured in endothelial cell growth medium (EGM Bullet Kit; Lonza, Cat. No. CC-3124) in

0.5% Matrigel, in the presence and absence of Deferoxamine mesylate salt (DFO used at 100 μM final concentration) (Sigma Aldrich, Cat. No. D9533-1G). Cells were maintained at 37°C in a humidified environment containing 5% CO_2 for 48 hours before tube formation was assessed. Moreover, we utilized FACS (as above) on our differentiated neurospheres to confirm the presence of murine tumor-derived endothelial cells ($CD31^+$, GFP^+).

References Cited:

1. Glasgow SM, Zhu W, Stolt CC, et al. Mutual antagonism between Sox10 and NFIA regulates diversification of glial lineages and glioma subtypes. *Nat Neurosci.* 2014; 17(10):1322-1329.

2. John Lin CC, Yu K, Hatcher A, et al. Identification of diverse astrocyte populations and their malignant analogs. *Nat Neurosci.* 2017; 20(3):396-405.

3. Yu K, Lin CJ, Hatcher A, et al. PIK3CA variants selectively initiate brain hyperactivity during gliomagenesis. *Nature.* 2020; 578(7793):166-171.

4. Cong L, Ran FA, Cox D, et al. Multiplex genome engineering using CRISPR/Cas systems. *Science.* 2013; 339(6121):819-823.

5. Xue W, Chen S, Yin H, et al. CRISPR-mediated direct mutation of cancer genes in the mouse liver. *Nature.* 2014; 514(7522):380-384.

6. Chen F, Rosiene J, Che A, Becker A, LoTurco J. Tracking and transforming neocortical progenitors by CRISPR/Cas9 gene targeting and piggyBac transposase lineage labeling. *Development.* 2015; 142(20):3601-3611.

7. Zudaire E, Gambardella L, Kurcz C, Vermeren S. A computational tool for quantitative analysis of vascular networks. *PLoS One.* 2011; 6(11):e27385.

8. Ricci-Vitiani L, Pallini R, Biffoni M, et al. Tumour vascularization via endothelial differentiation of glioblastoma stem-like cells. *Nature.* 2010; 468(7325):824-828.

9. Wang R, Chadalavada K, Wilshire J, et al. Glioblastoma stem-like cells give rise to tumour endothelium. *Nature.* 2010; 468(7325):829-833.

10. Ewels P, Magnusson M, Lundin S, Kaller M. MultiQC: summarize analysis results for multiple tools and samples in a single report. *Bioinformatics.* 2016; 32(19):3047-3048.

11. Patro R, Duggal G, Love MI, Irizarry RA, Kingsford C. Salmon provides fast and bias-aware quantification of transcript expression. *Nat Methods.* 2017; 14(4):417-419.

12. Love MI, Huber W, Anders S. Moderated estimation of fold change and dispersion for RNA-seq data with DESeq2. *Genome Biol.* 2014; 15(12):550.

13. Soneson C, Love MI, Robinson MD. Differential analyses for RNA-seq: transcript-level estimates improve gene-level inferences. *F1000Res.* 2015; 4:1521.

14. Ge SX, Jung D, Yao R. ShinyGO: a graphical gene-set enrichment tool for animals and plants. *Bioinformatics.* 2020; 36(8):2628-2629.

15. Sabbagh MF, Heng JS, Luo C, et al. Transcriptional and epigenomic landscapes of CNS and non-CNS vascular endothelial cells. *Elife.* 2018; 7.

16. Vanlandewijck M, He L, Mae MA, et al. A molecular atlas of cell types and zonation in the brain vasculature. *Nature.* 2018; 554(7693):475-480.

17. McInnes LH, J.; Melville, J. UMAP: Uniform Manifold Approximation and Projection for Dimension Reduction. *ArXiv e-prints.* 2018:arXiv:1802.03426.

18. Qiu X, Hill A, Packer J, Lin D, Ma YA, Trapnell C. Single-cell mRNA quantification and differential analysis with Census. *Nat Methods.* 2017; 14(3):309-315.

19. Qiu X, Mao Q, Tang Y, et al. Reversed graph embedding resolves complex single-cell trajectories. *Nat Methods.* 2017; 14(10):979-982.

20. Trapnell C, Cacchiarelli D, Grimsby J, et al. The dynamics and regulators of cell fate decisions are revealed by pseudotemporal ordering of single cells. *Nat Biotechnol.* 2014; 32(4):381-386.

21. Glasgow SM, Laug D, Brawley VS, et al. The miR-223/nuclear factor I-A axis regulates glial precursor proliferation and tumorigenesis in the CNS. *J Neurosci.* 2013; 33(33):13560-13568.

22. Soda Y, Marumoto T, Friedmann-Morvinski D, et al. Transdifferentiation of glioblastoma cells into vascular endothelial cells. *Proc Natl Acad Sci U S A.* 2011; 108(11):4274-4280.

23. Subramanian A, Tamayo P, Mootha VK, et al. Gene set enrichment analysis: a knowledge based approach for interpreting genome-wide expression profiles. *Proc Natl Acad Sci U S A.* 20005; 102(43):15545-15550.

24. Mootha VK, Lindgren CM, Eriksson K-F, et al. PGC-1alpha-responsive genes involved in oxidative phosphorylation are coordinately downregulated in human diabetes. Nat. Genet. 2003; 34(3):267-273.